

SEMMELWEIS EGYETEM
DOKTORI ISKOLA

Ph.D. értekezések

3185.

SVAJDA LAURA

Molekuláris és experimentális onkológia
című program

Programvezető: Dr. Bödör Csaba, egyetemi tanár

Témavezetők: Dr. Tóvári József, osztályvezető

Dr. Cserepes Tamás Mihály, biológus kutató

TARGETING TUMOR HYPOXIA IN COMBINED THERAPEUTIC STRATEGIES IN BREAST AND OVARIAN CANCER

PhD thesis

Laura Svajda

Semmelweis University Doctoral School
Pathological and Oncological Division



Supervisors:

József Tóvári, D.Sc

Mihály Cserepes, Ph.D

Official reviewers:

Anna-Mária Tőkés, Ph.D

Borbála Székely, MD, Ph.D

Head of the Complex Examination Committee: Gábor Lotz, MD, Ph.D

Members of the Complex Examination Committee:

Henriett Butz, MD, Ph.D

Katalin Erdélyi, Ph.D

Budapest

2025

Table of contents

List of Abbreviations	4
1. Introduction	7
1.1. Epidemiology, incidence, and mortality of breast and ovarian cancers	7
1.2. Therapeutic strategies against breast and ovarian cancers.....	9
1.3. Root causes of mortality in cancer patients	10
1.4. The components and impact of tumor microenvironment.....	12
1.5. The role of tumor hypoxia in tumor progression	14
1.6. Tumor hypoxia as a druggable target.....	15
1.7. Strategic approaches – combination therapies.....	18
2. Objectives.....	19
3. Methods.....	20
3.1. Cell culturing	20
3.2. Therapeutic agents	20
3.3. Hypoxia modeling.....	20
3.4. Antiproliferative assessment of single and combinatorial drug effects	21
3.5. Drug-drug interaction analysis.....	21
3.6. NDRG1 mRNA expression detection by qPCR	21
3.7. Western blotting.....	22
3.8. Sample processing for proteomic analysis.....	23
3.9. Nano-scale liquid chromatographic tandem mass spectrometry analysis.....	23
3.10. Wound healing assay.....	25
3.11. <i>In vivo</i> hypoxia model establishment.....	25
3.12. <i>In vivo</i> toxicity and efficacy	26
3.13. Histology	27
3.14. Immunohistochemistry (IHC) analysis of tumor microarrays (TMA).....	27
3.15. Statistical analysis	27
4. Results	28
4.1. Antiproliferative assessment of acriflavine	28
4.2. Proteomic profile alterations induced by hypoxic and acriflavine treatment ...	30
4.3. Molecular analysis of <i>in vitro</i> hypoxia induction and inhibition.....	35
4.4. Interaction assessment of acriflavine and paclitaxel.....	37
4.5. Migratory assessment of the combination treatment	40
4.6. Assessment of the <i>in vivo</i> hypoxia-inducible impact of CoCl ₂	41

4.7.	<i>In vivo</i> safety and efficacy evaluation of the drug combination	42
4.8.	Molecular analysis of the orthotopic xenografts.....	44
4.9.	HIF-1 α and PD-L1 co-expression assessment	46
5.	Discussion	48
6.	Conclusion.....	53
7.	Summary	55
8.	References	56
9.	Bibliography of the candidate's publications.....	66
9.1.	Publication related to the thesis	66
9.2.	Other publications	66
10.	Acknowledgments	68
11.	Grant support	69

List of Abbreviations

ABC	ATP-binding cassette
ACF	Acriflavine
AKT	Protein kinase B
BC	Breast cancer
BSA	Bovine serum albumin
BRCA	Breast cancer gene
CAA	Cancer-associated adipocyte
CAF	Cancer-associated fibroblast
CDK4/6	Cyclin-dependent kinase 4 and 6
CoCl ₂	cobalt (II)-chloride
CTLA-4	Cytotoxic T-lymphocyte-associated protein 4
DMEM	Dulbecco's Modified Eagle's Medium
ECAD	E-cadherin
ECM	Extracellular matrix
EGFR	Epidermal growth factor receptor
EMT	Epithelial-mesenchymal transition
ER	Estrogen receptor
ERK	Extracellular signal-regulated kinase
FDR	False discovery rate
HIF	Hypoxia-inducible factor
HRE	Hypoxia-response element
HER2	Human epidermal growth factor receptor 2
HR	Hormone receptor
HRD	Homologous recombination deficiency
HRP	Horse-radish peroxidase
HSP90	Heat shock protein 90
ICI	Immune checkpoint inhibitors
IHC	Immunohistochemistry

IL-2	Interleukin-2
LDHA	Lactate dehydrogenase A
MAPK	Mitogen-activated protein kinase
MEK	Mitogen-activated extracellular signal-regulated kinase
MMP	Matrix metalloproteinase
MSC	Mesenchymal stem cells
mTOR	Mammalian target of rapamycin
NOD-SCID	NOD.CB17-Prkdcscid/NCrCrI
nLC-MS/MS	Nano-scale liquid chromatographic tandem mass spectrometry
NDRG1	N-myc downstream regulated 1
PARP	Poly (ADP-ribose) polymerase
PBS	Phosphate-buffered saline
PD-1	Programmed cell death protein 1
PD-L1	Programmed cell death ligand 1
PI3K	Phosphoinositide 3-kinase
PHD2	Prolyl hydroxylase domain-containing protein 2
PR	Progesterone receptor
qPCR	Quantitative real-time polymerase chain reaction
R	Rolipram
RPLP0	Ribosomal protein lateral stalk subunit P0
Rho GTPase	Ras homolog guanosine triphosphatase
SEM	Standard error of the mean
SRB	Sulforhodamine-B
OC	Ovarian cancer
PC	Pericyte
PTX	Paclitaxel
TAM	Tumor-associated macrophage
TGF- β	Transforming Growth Factor beta
TNBC	Triple-negative breast cancer

TMA	Tumor microarray
TME	Tumor Microenvironment
TEC	Tumor endothelial cell
T _{reg}	Regulatory T cell
VEGF	Vascular-endothelial growth factor
VHL	Von Hippel-Lindau protein

1. Introduction

1.1. Epidemiology, incidence, and mortality of breast and ovarian cancers

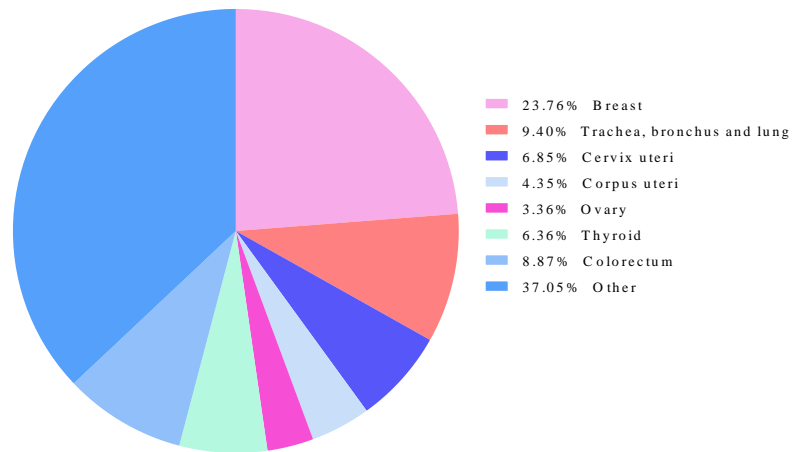
Cancer incidence covered nearly twenty million people globally in 2022 according to the estimates of the Global Cancer Observatory (1). The fatal outcomes account for almost half of this number, which promotes cancer among the most common death causes worldwide, besides cardiovascular diseases. Lung, colorectal, liver, breast, stomach, and pancreas cancers account for more than half of these mortal cases. At the same time, other enteral, gynecological, urological, head-and-neck regions, nervous system, and hematological malignancies take out the rest of the mortalities. Lung cancer alone caused 18% of all cancer deaths, which was consistent with its highest incidence rate (12%) in both sexes. Following the malignancies of the lung, breast cancer (BC) is the second most common subtype of cancer when considering the total population and first when taking into account female patients only (1).

Despite the high incidence of breast cancer of all cancers in the female population (23.8%), the constantly emerging therapeutic options reduced the mortality of the disease (2). However, breast cancer is still the leading cause of death among women suffering from cancer (1). Comparing the incidence of ovarian cancer (OC) with breast cancer and other gynecological malignancies, a significantly lower incidence rate was observed (3.4%). However, the low incidence of ovarian cancer is responsible for nearly 5% of all cancer deaths in the female population (**Figure 1A-B**). According to the National Cancer Registry and the Hungarian Central Statistical Office, approximately 8000 new cases of breast cancer and around 1400 cases of ovarian cancer are diagnosed annually among women in Hungary. The mortality rates are approximately 2100 and 700, respectively (3).

Considering the high incidence of breast-, and the high mortality of ovarian cancers we opted to develop novel therapeutic strategies against these malignancies. In the next chapter, the currently available pharmacological approaches are introduced.

A

Global cancer incidence in female cancer patient population



B

Global cancer mortality in female cancer patient population

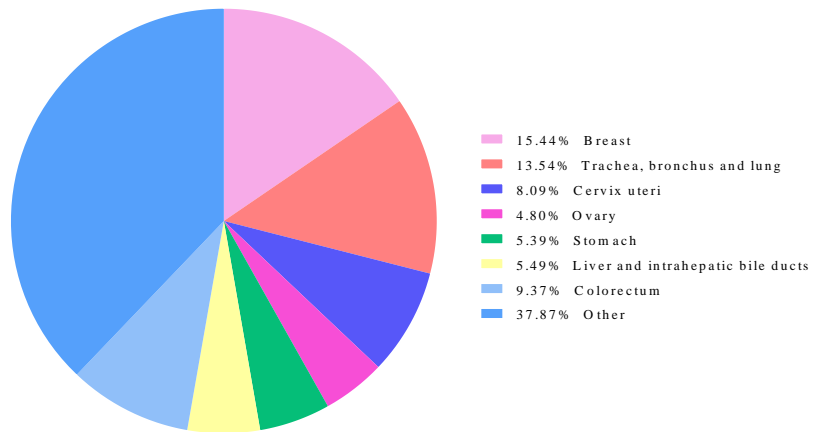


Figure 1. Global cancer incidence (**A**) and mortality (**B**) in the female cancer patient population focusing on the cancer types with the highest incidence rate based on the database of Global Cancer Observatory 2022. Percentage values were calculated by considering all cancer cases 100% (4).

1.2. Therapeutic strategies against breast and ovarian cancers

Besides surgical intervention and irradiation, a wide range of medical agents are available for the treatment of breast and ovarian cancers. Among these, several compounds function as traditional cytostatic agents, while others belong to the targeted therapies subgroup. Targeted therapies serve as novel therapeutic strategies for selective cancer treatment by targeting single moieties involved in essential cellular pathways on cancer cells (5). Several advantages stand for these options such as decreased systematic toxicity, and moderate side effects. However, these therapies cannot express their function when cancer cells lack a druggable target. Moreover, upon eliminating tumor cells carrying the target molecules, a remaining subpopulation of cells lacking the target repopulates a more aggressive, often therapy-resistant tumor. Despite these limitations, combining targeted therapies with traditional cytostatic agents represents a possible solution to overcome this issue, but it is not fully followed in clinical practice (6).

Breast cancer treatment is subtype-dependent. Patients with tumors overexpressing human epidermal growth factor 2 (HER2) usually receive trastuzumab and pertuzumab mono- or combination therapies. In more advanced cases, trastuzumab-deruxtecan and tucatinib are involved (7). In the case of hormone receptor (HR) expressing tumors, endocrine therapies such as estrogen receptor modulators (e.g., tamoxifen) and aromatase inhibitors (e.g., letrozole) are applied (8). Cyclin-dependent kinases 4 and 6 (CDK4/6) inhibitors such as ribociclib or palbociclib achieved significant progression in treating metastasized, hormone-receptor-positive cases (9).

When tumor cells lack a druggable target, for instance, in the case of triple-negative breast cancer (TNBC), the treatment options are limited. In TNBC, besides cytotoxic chemotherapeutics such as cisplatin or paclitaxel (PTX) are applied. The involvement of poly (ADP-ribose) polymerase (PARP) inhibitors (e.g., olaparib) in the treatment of breast cancer gene (BRCA) mutation harboring TNBC patients led to significant improvements by increasing progression-free survival (10–12).

In the treatment of ovarian cancer, platinum-based therapies (e.g., carboplatin) are commonly applied either as monotherapy or in combination with other chemotherapeutics such as paclitaxel. In platinum-resistant cases, liposomal doxorubicin, gemcitabine, etoposide, and topotecan are used. PARP inhibitors are widely involved in ovarian cancer

treatment, especially in platinum-sensitive, BRCA-mutant, and homologous recombination deficiency (HRD) positive cases. The low oxygenation affects both breast and ovarian tumors, which leads to the formation of unmaturing blood vessels by enhanced angiogenesis (12,13). Therefore, administering a vascular endothelial growth factor inhibitor, bevacizumab is reasonable in both BC and OC treatment (14,15).

A recent advancement in cancer therapy is the incorporation of immune checkpoint inhibitors (ICIs) in treatment regimens. ICIs are monoclonal antibodies that aim to lift the inhibitory pathways between immune cells and cancer cells to enhance T-cell-mediated anti-tumor immune responses. These antibodies either target the blockade generated by the programmed cell death protein 1 (PD-1) receptor and its ligand, the programmed death ligand 1 (PD-L1), or by the cytotoxic T-lymphocyte-associated protein 4 (CTLA-4). In breast cancer, ICIs have shown efficacy primarily in TNBC, where anti-PD-1/PD-L1 therapies, such as atezolizumab and pembrolizumab, improved progression-free survival (16). In ovarian cancer, despite initial promise, ICIs have demonstrated limited clinical benefit as monotherapy, but ongoing research explores their potential in combination with chemotherapy, anti-angiogenic agents, and PARP inhibitors (17).

1.3. Root causes of mortality in cancer patients

Several factors interplay behind the high mortality of cancer. The major contributor to the lethal outcome of the disease is metastasis formation. It occurs upon tumor cells migrating from the primary tumor site to distant organs (18). This process is promoted by environmental factors, genetic mutations, gene expression alterations, growth factor release, and enhanced angiogenesis contributing to intravasation. When entering blood vessels tumor cells are exposed to high shear stress, however, the stem-cell-like characteristics and platelet cloaking promote survival in the circulation. When tumor cells reach the vasculature of distant organs, they adhere to endothelial cells and then extravasate to colonize the organ (**Figure 2.**). Metastases formed this way may exhibit different genetic backgrounds comparing primary tumors, often resulting in more aggressive phenotypes (19–21).

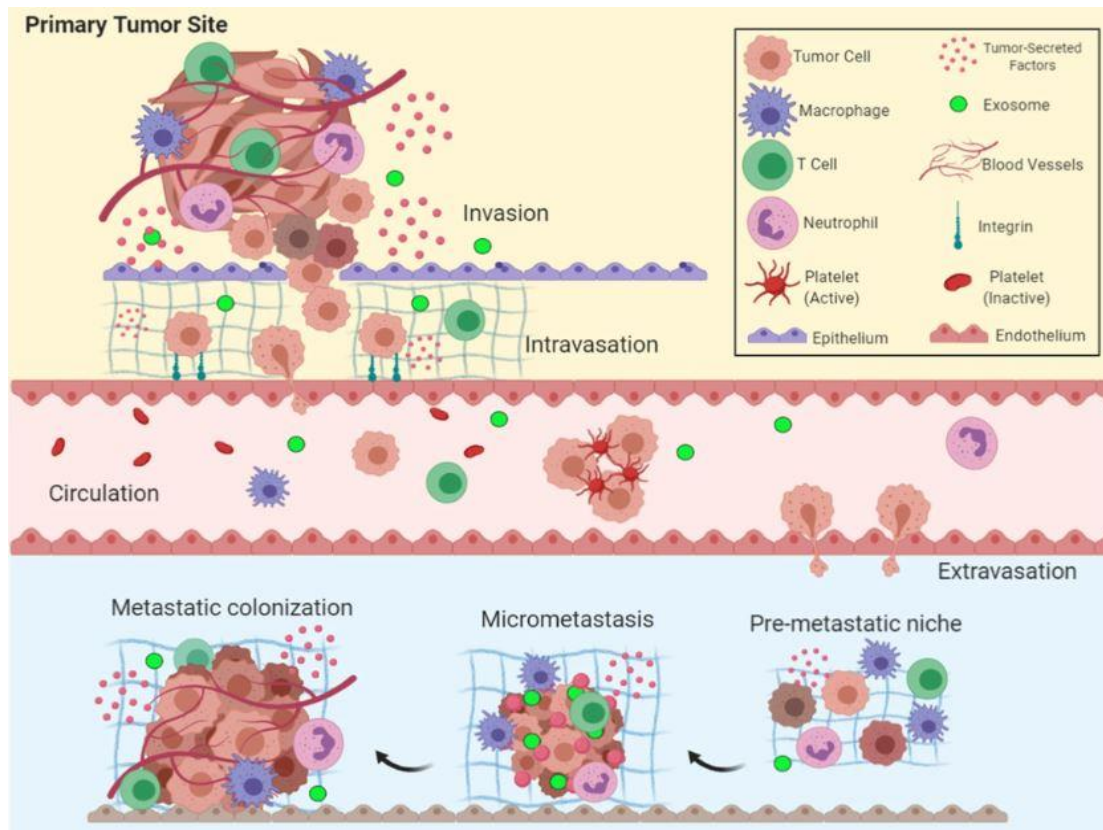


Figure 2. Schematic representation of metastasis formation (invasion, intravasation, circulation, extravasation, and colonization) including the cellular components of the tumor microenvironment This figure was adapted from Fares et al. (22).

Both breast and ovarian cancers tend to metastasize frequently. Breast tumor cells preferentially spread to surrounding lymph nodes, bones, liver, lung, and brain (23). The most common metastatic sites of ovarian cancer include the peritoneum, liver, and lymph nodes. Moreover, metastatic ovarian cancer might affect the bones and the brain as well (24). Consequently, metastasized disease encounters lower life expectancy, especially in the case of OC patients. Therefore, novel therapeutic strategies are essential to overcome disease progression.

Although metastasis is a major contributor to cancer-related mortality, additional classifications of acute and underlying causes of death have been described. Cancer-related vascular and cardiac complications, tumor mass-caused impaired organ functions, infections, paraneoplastic syndromes, and therapeutic toxicity are associated with cancer-related acute death. Meanwhile, as underlying cancer-related death causes, the impeded

immune functions, the reprogrammed metabolism, and the corresponding cachexia are mentioned (25).

As metastasis formation significantly contributes to cancer progression, it decreases life expectancy. Therefore, the absolute necessity of early-stage diagnosis is emphasized. On the other hand, accounting for metastasis preventive measures are obliged elements of cancer treatment regimens.

1.4. The components and impact of tumor microenvironment

A significant achievement of the past decade is the incorporation of immune checkpoint inhibitors into cancer treatment. Along with angiogenesis inhibitors and matrix metalloproteinase (MMP) modulators (26), these innovative therapeutics have driven a revolution in cancer therapy, bringing increasing research interest in the impact of the tumor microenvironment (TME) on tumor progression and metastasis. Moreover, considering the interactions of TME with the host and the tumor, the targetability of TME has appeared as an effective cancer treatment strategy (27). TME-targeting therapies, including anti-angiogenic agents, hypoxia inhibitors, extracellular matrix modulators, and metabolic pathway inhibitors, show potential in inhibiting tumor progression, however, their efficacy is often limited by adaptive resistance mechanisms (28).

TME includes tumorous and non-tumorous cells and non-cellular components (**Figure 2.**). Stromal and immune cells are non-malignant cellular representatives of the TME. Stromal cells, such as cancer-associated fibroblasts (CAFs), mesenchymal stem cells (MSCs), tumor-associated adipocytes (CAAs), tumor endothelial cells (TECs), and pericytes (PCs) make up the vast majority of the cellular elements. Stromal cells are responsible for metabolic alterations, growth, metastasis, immune evasion, and treatment resistance. CAFs produce fibronectin and collagen, secrete cytokines and growth factors, and hence contribute to the growth, proliferation, invasion, and migration of tumor cells. MSCs foster tumor-promoting signal-transduction pathways and can transform into tumor-promoting cells, induce angiogenesis, and enhance epithelial-mesenchymal transition (EMT). EMT promotes migration, thereby metastasis formation, by stimulating the change between epithelial and mesenchymal phenotypes (29). When undergoing EMT, the epithelial form loses epithelial features and gains mesenchymal properties, promoting migration (30). TECs are involved in angiogenesis, forming new blood vessels

and thus providing nutrition and oxygen to the tumor mass. By secreting cytokines, lipid metabolites, adipokines, and exosomes, CAAs contribute to proliferation, immune suppression, and EMT. PCs are responsible for immune regulation by enhancing the accumulation of tumor-associated macrophages (TAMs) and regulatory T cells (T_{reg}) and inhibiting $CD8^+$ cell infiltration (29). TAMs, being important representatives of immune cells of TME, suppress the adaptive immune response and promote angiogenesis by producing vascular endothelial growth factor (VEGF). Natural killer (NK) and dendritic cells often encounter loss of function, making them incapable of tumor cell elimination or antigen presentation (31–33).

The non-cellular component of TME is the extracellular matrix (ECM), a complex structure consisting of collagens, proteoglycans, and glycoproteins. ECM is a dynamic system that serves as a mechanical support for the cells. Tumor cells are capable of reshaping the ECM through enzyme production, leading to ECM digestion and, thus, enhanced motility (34).

In summary, tumor cells efficiently interact with other non-tumorous cellular components of the TME via complex cascades. These complicated networks are still not fully revealed, however, novel research techniques such as single-cell sequencing may contribute to deeper understanding. Recognizing the impact of the TME on tumor progression, several drug candidates have been developed to target the microenvironmental components (29).

1.5. The role of tumor hypoxia in tumor progression

Tumor hypoxia is a common feature of solid tumors and a determining factor of tumor environment. The rapid proliferation of tumor cells leads to elevated oxygen and nutrient demand (35). However, the inadequate vasculature of solid tumors is often incapable of supplying this. Angiogenic factors produced by CAFs promote angiogenesis, resulting in rapid formation of unmaturing, impaired blood vessels (29). The inability to properly transfer oxygen leads to oxygen-deprived areas in the tumor mass. To adapt to this unfavorable, hypoxic environment, tumor cells switch on a specific program enhancing their survival.

The key factor of the adaptation to poor oxygenation is the hypoxia-inducible factor 1 (HIF-1). HIF-1 is a transcription factor consisting of two subunits, an α , and a β , and its activation depends on the stability of the α subunit (36). While the β subunit is constitutively active, the stabilization of the α subunit is oxygen-dependent. If the tissue is well-oxygenated the prolyl hydroxylase domain-containing protein 2 (PHD2) is active to label HIF-1 α for ubiquitination by the von Hippel-Lindau (VHL) tumor suppressor and subsequent degradation by proteasomes. However, in the hypoxic environment, the activity of the prolyl-hydroxylase enzymes is inhibited, leading to HIF-1 α stabilization and nucleus translocation. Upon dimerization in the nucleus with the β subunit, a transcriptionally active HIF-1 complex is formed, which binds to the hypoxia-responsive elements (HRE) of the promoter region of nearly 100 target genes, supporting their transcription. Consequently, HIF-1 is responsible for the activation of numerous gene cascades, involved in angiogenesis, proliferation, growth, survival, migration, invasion, and immune suppression (37–39).

Even though the activation of the HIF-1 transcription factor is oxygen-sensitive, oxygen-independent activation was also described. Alterations in important cell-signaling pathways (e.g., MAPK/ERK, PI3K) and tumor suppressor proteins (e.g., p53) may trigger the HIF-1 cascade, promoting the survival of tumor cells (40–42).

HIF-1 α mitigates the immune system, by enhancing the expression of PD-L1. PD-L1 then binds to its receptor, resulting in suppressed T cell function. Moreover, HIF-1, by facilitating the transcription of lactate dehydrogenase A (LDHA) creates an acidified tumor environment which impairs the function of immune cells. Additionally, HIF-1

affects the function of drug-efflux proteins and induces ATP-binding cassette (ABC) transporter overexpression, hence stimulating resistance development against chemotherapies and ICIs (43,44).

1.6. Tumor hypoxia as a druggable target

Based on the database of The Cancer Genome Atlas (TCGA), we have previously analyzed the potential effect of HIF-1 mRNA expression on the overall survival of BC and OC patients (45,46). Interestingly, by assessing the survival probability by HIF-1 α activation through the mRNA expression of an important HIF-1 target, N-myc downstream-regulated 1 (NDRG1), a notable correlation was identified in BC, however, this was not present in OC (**Figure 3.**). Thus, considering the underlying gene cascade of HIF-1 activation and how it affects the survival of patients with breast and ovarian cancers, the transcription factor is an attractive drug target.

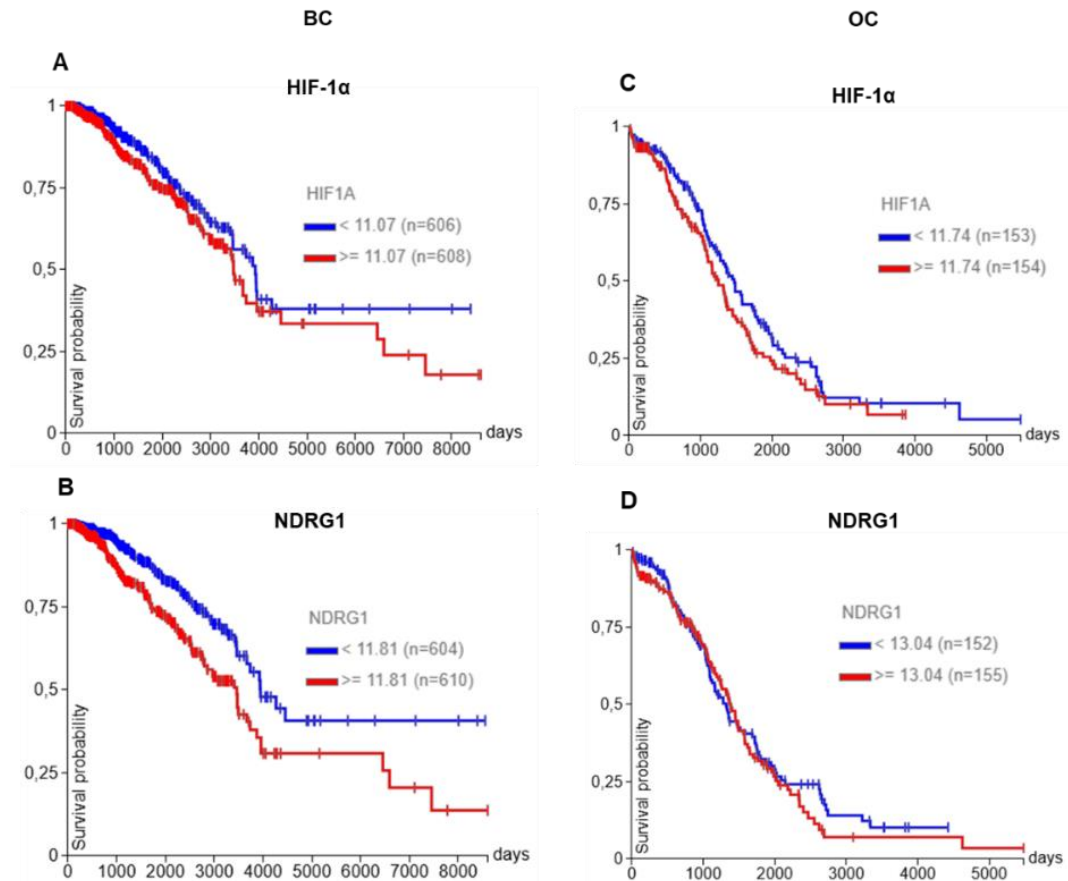


Figure 3. The impact of the mRNA expression profile of HIF-1 and NDRG1 on the overall survival in breast and ovarian cancers (BC and OC respectively). Survival probability in the context of HIF-1 α and NDRG1 mRNA expression in BC (**A-B**) and OC (**C-D**). Kaplan-Meier plots were generated by the Xena platform (University of California) based on The Cancer Genome Atlas (TCGA) Breast and Ovarian Cancer Databases and gene expression datasets. The p values were as follows: **A:** $p=0.038$; **B:** $p=0.000037$; **C:** $p=0.1035$, **D:** $p=0.4840$. The figure was adapted from the author's original publication (45,46).

Several HIF-1 inhibitors with different mechanisms of action were developed in the previous decades (**Figure 4**). Most commonly, these drugs, such as chetomin, echinomycin, and epirubicin target the transcriptional activity of HIF-1 (47–49). Others, like YC-1 or digoxin, inhibit the translation of the α subunit (47,50). Radicol and romidepsin impede HIF-1 α stabilization by inhibiting heat shock protein 90 (HSP90) and histone deacetylase, respectively (47). Rapamycin and everolimus were identified as PI3K pathway modulators and indirect HIF-1 inhibitors (50). Acriflavine (ACF), – known

as dual inhibitors of HIF-1 and HIF-2 – is a widely used antiseptic agent that hinders the dimerization of the subunits (51).

Even though the promising preclinical results, the HIF1- inhibitors serially failed in Phase II trials. The root causes were the lack of efficacy and the resistance mechanisms (52,53). Additionally, the high toxicity, the pharmacokinetic and dynamic barriers, and the compensatory mechanisms generated by HIF-2 and HIF-3 further hampered the success (54). On the contrary, the application of belzutifan, a HIF-2 inhibitor, was accepted for renal cell carcinoma and VHL mutation-related diseases (55).

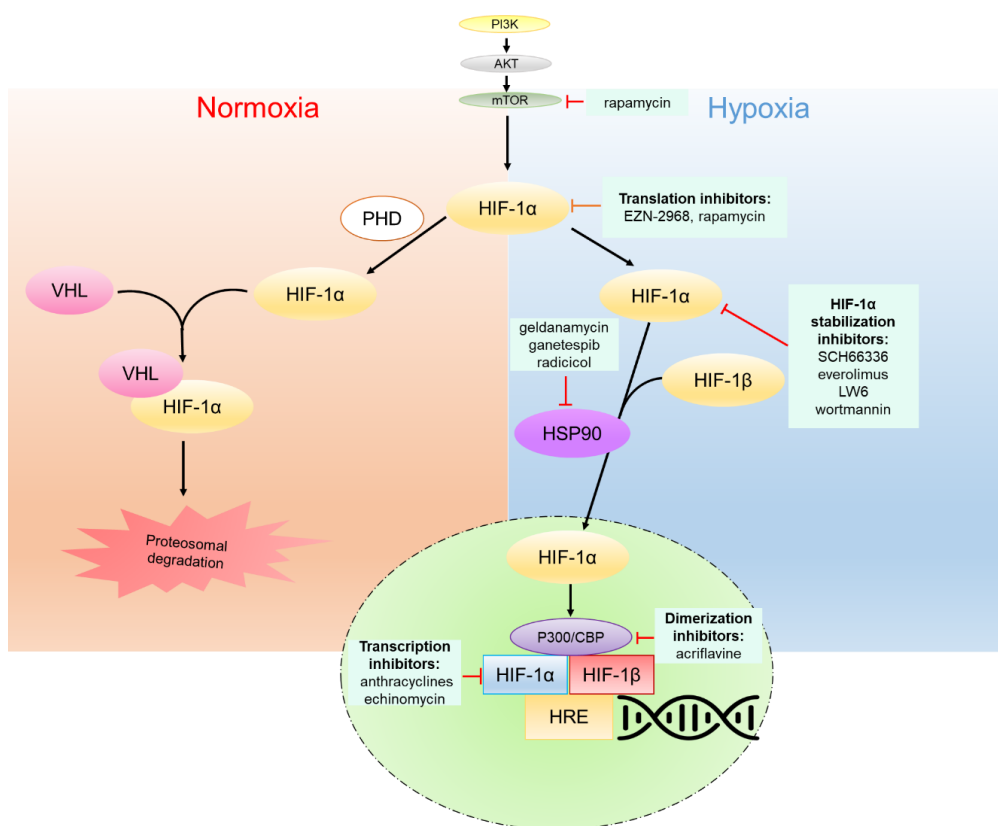


Figure 4. The mechanism of action of HIF inhibitors. The figure was adapted from the author’s original publication (46).

1.7. Strategic approaches – combination therapies

Targeting HIF-1 is essential to prevent metastasis formation and immune suppression, and due to the failure of HIF-1 inhibitor monotherapies, an absolute need for a strategic solution is inevitable. Combined therapeutic approaches were considered to overcome the limitations of HIF-1 inhibitor monotherapies. Importantly, combining HIF-1 inhibitors with conventional chemotherapeutic agents and kinase inhibitors increased the efficacy of the treatments (56). Moreover, successful studies were published about the simultaneous application of ICIs and HIF-1 inhibitors (57,58).

2. Objectives

The general objective of the research was to study the hallmark of hypoxia, and the impact of an oxygen-deprived environment on tumor progression. Another goal was to circuit possible ways to target tumor hypoxia, the underlying pathways, and the microenvironment.

In this study we aimed to:

- (1) Study the impact of tumor hypoxia on crucial cellular processes and set up a suitable *in vitro* testing system for multidrug studies.
- (2) Investigate the efficacy and safety of the combination of acriflavine and paclitaxel in *in vitro* and *in vivo* systems.
- (3) Address hypoxia-related alterations and the compensatory effect of the drugs on tumor cell proliferation, migration, invasion, and metabolism.
- (4) Observe the possibilities of indirect EMT targeting.
- (5) Analyze the rationale behind simultaneously applying HIF-1 inhibitors and ICIs.

3. Methods

3.1. Cell culturing

Seven subtypes of BRCA-wild type (59–61) breast -and ovarian cancer lines obtained from the American Type Culture Collection (ATCC) with passage numbers lower than 30 were selected for the *in vitro* experiments. Among breast cancer cell lines, three TNBCs – MDA-MB-231, HS578T, 4T1 – and one HER2+ ER- PR-, MDA-MB-453 were used. Of ovarian cancer cell lines, we involved OVCAR-8 (HER2+ ER+ PR-), SKOV-3 (HER2+ ER+ PR-) and OVCAR-3 (HER2+ PR+ HR+). Six of the seven cell lines are human, while one, 4T1, is a murine cell line. Cells were incubated at either atmospheric (normoxia, 21%) or at 1% oxygen level (hypoxia), at 37°C next to 5% CO₂ level. 1% oxygen level was achieved by automatized N₂ injection in Esco CelCulture® CCL-170T-8 CO₂ & O₂ control incubator (Esco Lifesciences Group, Singapore). As growth medium, depending on cellular preference, either DMEM (Dulbecco's Modified Eagle's Medium, BioSera, Nuaille, France) or RPMI1640 (BioSera) cell culture medium completed with 1% penicillin/streptomycin (BioSera) and 10% fetal bovine serum (BioSera) was applied. Cells were maintained in T25 or T75 sterile, ventilated flasks (Sarstedt, Nümbrecht, Germany) and, if confluency reached 90% were exposed to trypsinization (BioSera), then were reseeded in 1:6 or 1:8 ratio.

3.2. Therapeutic agents

Acriflavine (#A12252) and paclitaxel were purchased from AdooQ (Irvine, CA) and TEVA Pharmaceuticals (Parsippany, NJ), respectively. Rolipram (#HY-16900) was supplied by Medchemexpress (Monmouth Junction, NJ). Cobalt (II)-chloride (CoCl₂) was purchased from Sigma-Aldrich (#60818, Burlington, MA).

3.3. Hypoxia modeling

Modeling tumor hypoxia was established by incubating the cells either at 1% oxygen concentration or by applying CoCl₂ in the cell culturing medium. CoCl₂, a prolyl hydroxylase inhibitory compound chemically induces hypoxia by stabilizing HIF-1 α . In *in vivo* systems, we aimed to achieve tumor hypoxia by administering 200 mg/liter CoCl₂ in drinking water.

3.4. Antiproliferative assessment of single and combinatorial drug effects

The antiproliferative activity of acriflavine was assessed by Sulforhodamine B (SRB) assay. Cells were seeded in 4000-7000 cell/well density 24 hours before the treatment in 96-well plates (Sigma-Aldrich) containing 100 μ l completed medium followed by an overnight incubation at 37 °C. On the next day, acriflavine was applied in serum-free medium with a 9-point dilution series starting from 100 μ M, with a dilution factor of 5. 72 hours later SRB assay was performed as previously stated (62). Absorbance was measured at 570 nm by Tecan Spark® Multimode Microplate Reader (Tecan Group Ltd., Männedorf, Switzerland). The combined effect of acriflavine and paclitaxel was measured by SRB assay as well. 0, 200, 400, 600, 800, and 1000 nM acriflavine was combined with a 4-point dilution series of paclitaxel (10000; 39.06; 2.4; 0.15 nM) on a 96-well plate, then incubated for 72 hours under normoxia and hypoxia. The SRB measurements were repeated three times with technical triplicates, and then half-maximal inhibitory concentration (IC₅₀) values were calculated using GraphPad Prism 6 software (GraphPad, La Jolla, CA).

3.5. Drug-drug interaction analysis

The drug-drug interactions were assessed by SynergyFinder 3.0 (Helsinki, Finland) according to the user guide of the software (63). Baseline corrections were applied and the synergy score was calculated by the Loewe method. The synergy score (δ) refers to the drug-drug interactions: antagonistic if less than -10, additive if between -10 and +10, and synergistic if greater than +10.

3.6. NDRG1 mRNA expression detection by qPCR

Frozen kidneys were disintegrated by using a mortar under liquid nitrogen. Then, the frozen powder was dissolved in TRIzol Reagent (ThermoFisher Scientific, Waltham, MA). RNA was isolated by Direct-zol RNA Miniprep Plus (Zymo Research, Tustin, CA) kit according to the manufacturer's protocol. The concentration and the purity of the RNA were determined using NanoDrop One (ThermoFisher Scientific). RNA was reverse-transcribed to cDNA by the Reverse Transcription System kit (Promega Corporation, Madison, WI). Quantitative real-time PCR reactions were performed using SsoAdvanced Universal SYBR Green Supermix (Bio-Rad, Hercules, CA) with CFX96 Real-Time System. The primers were ordered from Sigma Aldrich. The mRNA expression was

analyzed by the $2^{-[\Delta\Delta Ct]}$ method using internal control, ribosomal protein lateral stalk subunit P0 (RPLP0).

3.7. Western blotting

2×10^5 MDA-MB-231 cells were seeded in 6-well plates, and then 24 hours later 0.5 μ M acriflavine treatment was applied in the growth medium. Subsequently, cells were incubated for 48 hours under hypoxia, or under normoxia either with or without 50 μ M CoCl_2 . Cells were washed with PBS then were fixed with 6% trichloroacetic acid (60 min, 4 °C), then were collected and centrifuged (6000 x g, 15 min, 4 °C). The supernatant was discarded then the precipitated protein was dissolved in a modified Laemmli-type buffer containing 0.02% bromophenol blue, 10% glycerol, 2% sodium dodecyl sulfate, 100 mM dithiothreitol, 5 mM EDTA, 125 mg/ml urea, 90 mM Tris-HCl, pH 7.9. The protein concentration was determined by using a Qubit fluorometer (Invitrogen, Waltham, MA). The frozen tumor samples were disintegrated, and then the frozen powder was kept in 6% trichloroacetic acid for an hour at 4 °C. The following steps were identical in tissue and cellular samples. Each protein sample underwent sonication and then stored at -80 °C until further use. 10% Mini-Protean TGX Stain-free gels (Bio-Rad) were applied for electrophoresis. In each lane, an equal amount of 30 μ g total protein was measured. After electrophoresis, the samples were blotted on nitrocellulose membrane using the Trans-Blot Turbo Transfer System (Bio-Rad). The following antibodies were used: HIF-1 α (reference: ab51608, lot: GR3266947-4, Abcam, Cambridge, UK), E-cadherin (reference: 3195, lot: 15), and p-AKT (reference: 4060, lot: 25, Cell Signaling Technology: CST, Danvers, MA). Beta-Actin was used as the internal control (reference: A1978, lot: 0000180302, Merck, Darmstadt, Germany). The primary antibodies were diluted – HIF-1 α : 1:250; ECAD: 1:500, p-AKT: 1:500, Beta-Actin: 1:5000 – and then samples were incubated overnight at 4 °C. All primary antibodies were produced in rabbits, except for beta-actin, which was of mouse origin. Horse-radish-peroxidase (HRP) conjugated secondary anti-rabbit or anti-mouse antibodies (reference: 7074, lot: 28; reference: 7076, lot: 31, CST) were applied (1:1000 dilution, 1-hour, room temperature) then the signal was developed by the WesternBright ECL HRP substrate (12045, Advansta, San Jose, CA). The signal was visualized by the UVITEC Alliance Q9 Chemiluminescence Documentation System (UVITEC, Cambridge, UK). The signal was analyzed with a densitometric approach by Image Lab software (Bio-Rad).

3.8. Sample processing for proteomic analysis

2×10^5 4T1 cells/well were seeded in 6-well plates, then 24 hours later cells were treated with 0.5 μM acriflavine and incubated either at hypoxia or at normoxia for 48 hours. Protein was extracted by using a lysis buffer of 10 mM dithiothreitol, 0.2 w/v% dodecyl- β -D-maltoside in 100 mM triethylammonium bicarbonate. The samples were boiled at 95 °C for 10 min, then were sonicated using 20 cycles of 15 s on/off at 4 °C in the Bioruptor plus UCD-300 (Diagenode, Liege, Belgium). Protein amounts were determined by Pierce 660 nm Protein Assay with Ionic Detergent Compatibility Reagent (ThermoFisher Scientific). The proteins were digested using S-Trap™ 96-well plate following the instructions of the manufacturer (ProtiFi, Fairport, NY). Briefly, samples were alkylated with 50 mM iodoacetamide for 30 min in the dark at room temperature, followed by tryptic digestion in 50 mM triethylammonium bicarbonate (enzyme: substrate, 1:50) at 37 °C overnight. Before the peptide concentration measurement (Pierce Quantitative Colorimetric Peptide Assay, ThermoFisher Scientific), 5% trifluoroacetic acid was applied.

3.9. Nano-scale liquid chromatographic tandem mass spectrometry analysis

Before the nano-scale liquid chromatographic tandem mass spectrometry (nLC-MS/MS) analysis, the 4T1 samples were spiked with indexed retention time peptides. One μg of peptide solution per sample was injected into the nLC column and samples were run in randomized order.

The nLC-MS/MS analysis was performed on an Orbitrap Exploris 480 mass spectrometer (Thermo Scientific) coupled to a Vanquish Neo nano UPLC system (Thermo Scientific), with an EASY-Spray ion source (Thermo Scientific). Peptides were loaded onto an Acclaim PepMap 100 C18 (75 $\mu\text{m} \times 2 \text{ cm}$, 3 μm , 100 Å, nanoViper) trap column and separated on an Easy-spray PepMap RSLC C18 column (75 $\mu\text{m} \times 50 \text{ cm}$, 2 μm , 100 Å, Thermo Scientific) using a flow rate of 300 nL/min, and a column temperature of 60°C. A 90 min non-linear gradient was applied for separation, using solvents A (0.1% formic acid) and B (0.1% formic acid in 80% acetonitrile), increasing solvent B from 5 to 25% in 75 min, then to 32% in the next 9 min, and 45% in 6 min. Finally, the gradient increased to 95% solvent B in 2 min, continuing for another 8 min.

For data-independent acquisition, full MS resolution was set to 120000 (at 200 m/z), and the automatic gain control target value was 300% with a maximum injection time of 45 ms. The full MS mass range was set to m/z 350-1650. MS2 scans were acquired with a resolution of 45000, fragmentation with normalized collision energies of 27, 30, and 32, automatic gain control target value was set to 1000% with automatic injection time, fixed first mass of 200 m/z. Twenty-six variable isolation windows with an overlap of 1 m/z were used. MS raw files were analyzed using Spectronaut vs18.4 (Biognosys, Zurich, Switzerland) in library-free mode, using direct data-independent-acquisition factory default settings and MS2 quantification. The UniProt mouse protein database (UniProt, Cambridge, UK) with 17184 entries was used for the database search. Carbamidomethylation on cysteine and oxidation on methionine residues were considered as fixed and variable modifications, respectively. A maximum of two missed cleavages were allowed. A 1% false discovery rate (FDR) was applied both on peptide and protein levels. The raw protein intensities were log₂-transformed, and individual measurements were median normalized by centering their intensities around the global median. For statistical analysis, the expression table was filtered for proteins with a minimum of 50% valid values across samples, resulting in 5154 proteins. Missing value imputation was performed using impute.MinProb from the imputeLCMD R package (R Foundation for Statistical Computing, Vienna, Austria). Differential expression analysis was performed using the limma R package (R Foundation). Comparisons were done between hypoxic and normoxic conditions (hypoxia control versus normoxia control, hypoxia treated versus normoxia treated) and treated versus control cells (treated versus control in normoxia, treated versus control in hypoxia). Multiple testing correction was applied and FDR < 0.05 was considered significant. Heatmaps were plotted using the ComplexHeatmap R package (R Foundation). A principal component analysis biplot was drawn using the gg-biplot R package (R Foundation).

Pathway analysis was performed using the Database for Annotation, Visualization, and Integrated Discovery (DAVID) v6.8 (64,65) to identify significantly enriched pathways associated with up and downregulated genes. Differentially expressed proteins were first identified and categorized based on their expression levels under different experimental conditions. The corresponding gene lists were uploaded to DAVID for functional annotation and pathway enrichment analysis.

Enrichment was assessed using the Reactome database (Reactome, Toronto, Canada), focusing on pathways with an FDR-adjusted p-value < 0.05. The $-\log_{10}(\text{p-value})$ transformation was applied to enhance visualization, allowing for direct comparison of pathway significance. The top 10 upregulated and 10 downregulated pathways were selected for each experimental comparison and visualized as gradient-colored bar charts using the R `ggplot2` package (R Foundation).

3.10. Wound healing assay

MDA-MB-231 cells were seeded in 5×10^4 cell/well density in 96-well plate 24 h before the experiment. The wound was created by MuviCyte™ scratcher (PerkinElmer, Shelton, CT), then treatment was applied – 1 μM acriflavine, 0.0025 μM paclitaxel, 100 μM rolipram monotherapies, acriflavine+paclitaxel (double) and acriflavine+paclitaxel+rolipram (triple) combinations in the same concentrations. The cell migration was monitored by MuviCyte™ live-cell Imaging System (PerkinElmer) for 72 hours. The velocity of the wound closure was assessed by measuring the size of the wound every sixth hour using a modified script by ImageJ Fiji software (66).

3.11. *In vivo* hypoxia model establishment

Animal experimental procedures were approved and performed by the guidelines of the Institutional Animal Care and Use Committee at the National Institute of Oncology (Budapest, Hungary), under animal housing density regulations and recommendations from Directive 2010/63/EU of the European Parliament and the Council of the European Union on the protection of animals used for scientific purposes. Permission license for breeding and performing experiments with laboratory animals: PEI/001/1738-3/2015 and PE/EA/1461-7/2020. The animals used in this study were cared for according to the “Guiding Principles for the Care and Use of Animals” based upon the Helsinki Declaration and they were approved by the local ethical committee. The animal experiments were performed in compliance with ARRIVE guidelines. NOD.CB17-Prkdcscid/NCrCrl (NOD SCID) mice used in the study originated from the specified pathogen-free (SPF) animal house of the National Institute of Oncology. The mice were kept in a sterile environment in Makrolon cages (Akronom Ltd., Budapest, Hungary) at 22–24 °C (40–50% humidity), with a lighting regulation of 12/12 h light/dark. The animals had free access to water and were fed with a sterilized standard diet (VRF1,

autoclavable, Akronom) ad libitum. To test the hypoxia-inducible impact of CoCl₂ mice were treated over 21 days three times weekly in different administration routes: per os application by using an oral gavage (40 mg/kg) or by intraperitoneal injection (40 mg/kg). The third application route was ad libitum access by mixing CoCl₂ solution with drinking water (260 mg/l). Mice were terminated, and then kidneys were dissected and subjected to NDRG1 mRNA expression analysis by qPCR method.

3.12. *In vivo* toxicity and efficacy

The animals were anesthetized as previously described (67). 1x10⁶ MDA-MB-231 cells were inoculated in the mammary fat pad of female, approximately 20 g, 8-week-old NOD SCID mice. The tumor growth was followed by a caliper three times per week. Then, tumor volume was calculated by the following equation: Tumor volume = tumor (width² x length) x $\pi/6$. When tumors reached 50-70 mm³, mice were randomized and allocated into eight groups – every combination of acriflavine, paclitaxel, and CoCl₂. CoCl₂ – *in vivo* hypoxia inducer – was applied in 200 mg/liter mixed with drinking water ad libitum. Acriflavine and paclitaxel were administered intraperitoneally three times per week in 8 mg/kg and 5 mg/kg doses respectively for a period of 21 (CoCl₂) or 28 (no CoCl₂) days. Doses were established upon preliminary acute toxicity studies. During treatment, the body weight and the general condition of the mice were monitored regularly. After termination, the weight of the livers was measured and macrometastasis (>2 mm) occurrence was observed.

3.13. Histology

Livers were fixed in 8% formalin (Molar Chemicals, Halásztelek, Hungary), and then were embedded in paraffin blocks. Three-micrometer sections were stained with hematoxylin-eosin (H&E), then liver tissue alterations were observed in response to the applied drugs.

3.14. Immunohistochemistry (IHC) analysis of tumor microarrays (TMA)

Tumor microarray was produced by a partner research group, as stated elsewhere from different subtypes (Luminal A, Luminal B, Luminal B and HER2+, HER2+, TNBC) of freshly diagnosed, non-metastasized treatment naïve, breast tumors originating from female patients aged 30-90 years (68). To assess HIF-1 α expression on TMA, the immunohistochemistry method was performed by using HIF-1 α (reference: ab51608, Abcam) antibody in a dilution of 1:100 according to the method stated earlier (69). Ventana Ultraview DAB detection (Roche, Basel, Switzerland) kit was used according to the manufacturer's instructions, for the detection of the staining, followed by hematoxylin counterstaining. PD-L1 immunohistochemistry was conducted by the Ventana PD-L1 (SP142) Assay (Roche) according to the manufacturer's instructions by using Benchmark Ultra Plus (Roche) automatized system. Slides were scanned using Panoramic 250 Flesh III (3DHistech, Budapest, Hungary) slide scanner, then pictures were evaluated by the QuPath 0.5.1. software (70).

3.15. Statistical analysis

The statistical analysis was performed by GraphPad Prism 6 software. Both *in vitro* and *in vivo* data are presented by mean \pm standard error of the mean (SEM). Normality was tested with the Shapiro-Wilk test. One-way ANOVA and Tukey's multiple comparisons test were used for comparing mRNA and protein expression of each analyzed gene in response to the treatment. Two-way ANOVA and Sidak multiple comparison tests were applied to compare the effects of CoCl₂ for the analyzed genes. The tumor growth data and the results of the wound healing assays were evaluated by using the Kruskal-Wallis test. The p-values lower or equal to 0.05 were considered statistically significant.

4. Results

4.1. Antiproliferative assessment of acriflavine

To assess the antiproliferative activity of acriflavine under normoxic and hypoxic incubation (21% and 1% oxygen concentration, respectively), sulforhodamine B (SRB) assay was carried out on seven breast and ovarian cancer cell lines. After 72 hours of drug exposure and oxygen-depleted treatment, the cell viability was assessed and half-maximal inhibitory concentration (IC₅₀) values were calculated by nonlinear regression curve fitting. ACF functioned as a potent breast and ovarian cancer cell proliferation inhibitor, with the mean IC₅₀ of 700 nM and 1200 nM at normoxia and hypoxia respectively. Selectivity ratios were calculated by dividing the normoxic IC₅₀ values by the hypoxic IC₅₀ values. The highest selectivity ratios were observed in the case of MDA-MB-231 and HS578T TNBC cell lines, indicating the hypoxia-independent activity of the drug. Therefore, besides the human TNBC cell lines, a murine cell line, 4T1 was also analyzed. Acriflavine efficiently inhibited the proliferation of 4T1 cells, with a lower selectivity ratio than in the cases of human cells (**Figure 5., Table 1.**). For deeper mechanistic insight, we conducted proteomic analysis on the 4T1 cell line, ensuring the opportunity to use syngeneic models for *in vivo* validation that allows studying the immune aspects of tumor hypoxia.

Table 1. Breast and ovarian cancer cell lines involved in acriflavine efficacy assessment with IC₅₀ values and selectivity ratios under 72 h acriflavine treatment (N=3, mean ± SEM). The two highest selectivity ratios are bolded.

Type	Subtype	Cell line	Normoxia IC ₅₀ (nM)	Hypoxia IC ₅₀ (nM)	Selectivity ratio
					$\frac{\text{IC}_{50} \text{ Normoxia}}{\text{IC}_{50} \text{ Hypoxia}}$
Breast	TNBC	MDA-MB-231	520 ± 125	490 ± 23	1.1
	TNBC	HS578T	730 ± 125	970 ± 207	0.8
	TNBC	4T1	340 ± 160	560 ± 170	0.6
Ovarian	HER2+ ER- PR-	MDA-MB-453	660 ± 185	2080 ± 688	0.3
	HER2+ ER+ PR+	OVCAR-3	540 ± 166	780 ± 74	0.7
	HER2+ ER+ PR-	OVCAR-8	300 ± 18	590 ± 84	0.5
	HER2+ ER+ PR-	SK-OV-3	1430 ± 225	2730 ± 737	0.5

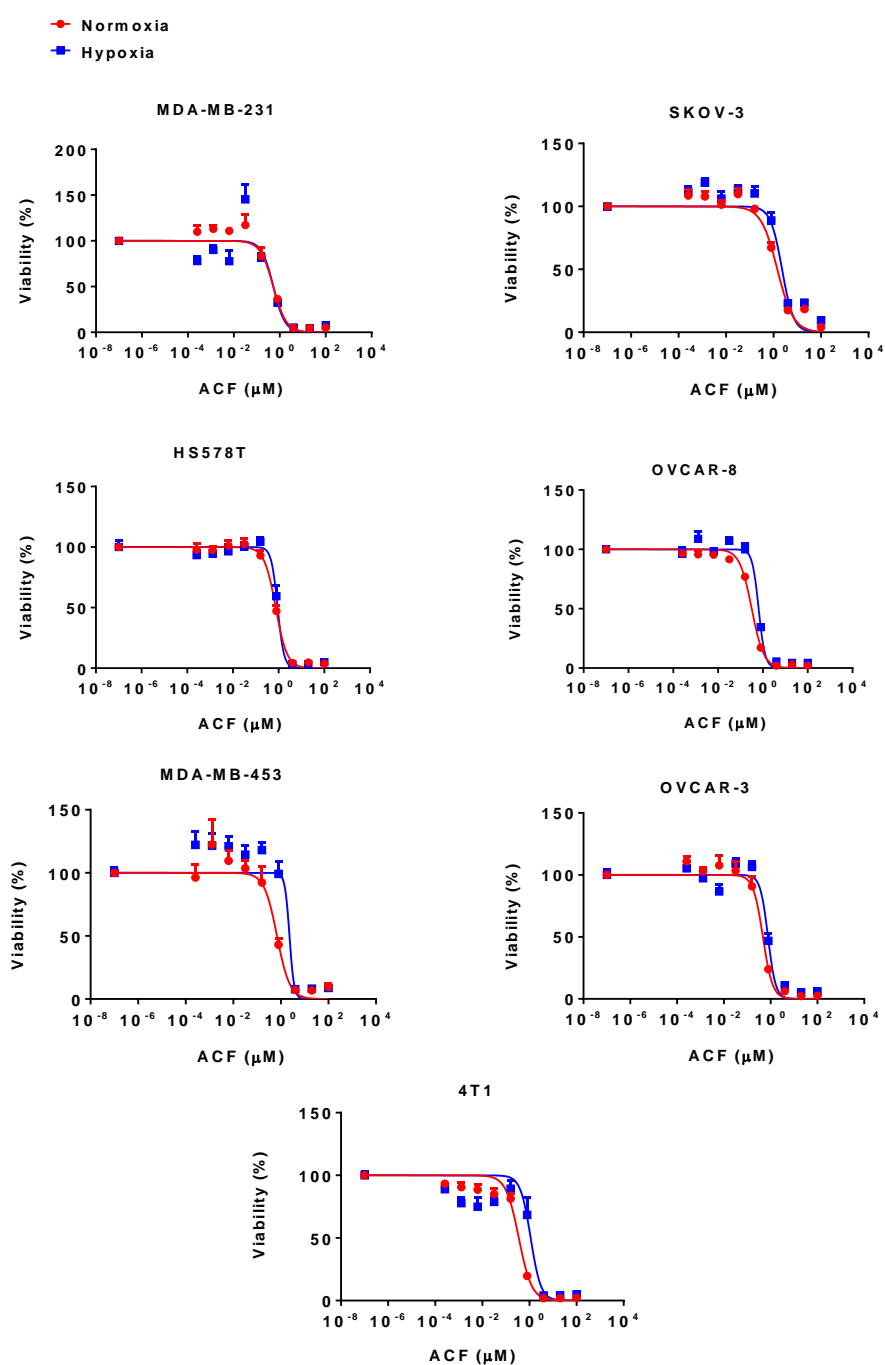


Figure 5. Cell line screening for acriflavine response. Illustration of the dose-viability correlation of the seven treated cell lines in response to 72 h acriflavine treatment. Data points represent mean + SEM, N=3, and curves are drawn using GraphPad Prism's non-linear fit (dose-response) module. The figure was adapted from the author's original publication (71).

4.2. Proteomic profile alterations induced by hypoxic and acriflavine treatment

To deeply understand the hypoxia-caused alterations in the proteomic profile, we conducted proteomic analysis on the 4T1 cell line. Moreover, proteomic profiling allowed us to investigate acriflavine's mechanism of action extensively.

A heatmap was drawn, based on the protein expression alterations in response to the different treatments. Notably, the hypoxic treatment caused elevated expression of several proteins, however, acriflavine treatment suppressed this impact. Interestingly, proteins that showed high expression in normoxia without acriflavine presented lower expression in response to ACF. Additionally, proteins with low expression profiles without ACF exhibited opposite outlines when treated with the drug (**Figure 6A**). Generally, when considering the effect of hypoxic treatment, we conclude that besides hypoxia triggers the expression of a notable amount of proteins, it is also responsible for downregulating an abundant group. Acriflavine caused protein downregulations under both normoxia and hypoxia, besides being responsible for upregulating a smaller group of proteins (**Figure 6B**). DAVID was used to assign the significantly altered genes into pathways. First, the upregulated pathways were assessed in response to hypoxic treatment. It notably increased the expression of genes involved in mitochondrial protein degradation, metabolism, cholesterol biosynthesis, β -oxidation of fatty acids, and extracellular matrix remodeling (**Figure 7A**). In response to acriflavine: kinesin, Ras homolog guanosine triphosphatase (Rho GTPase) signaling, vesicular transfer between Golgi and ER, and mitosis ana- and metaphases pathways were upregulated under normoxia. Consequently, it affected microtubule dynamics, cytoskeletal remodeling, intracellular trafficking, and mitotic regulation (**Figure 7B**). Rho GTPase signaling was also upregulated under hypoxia upon ACF treatment. Genes responsible for regulating the mitochondrial respiratory chain, and the metabolism of transferrin, iron, and glucose were overexpressed. ACF interfered with cell proliferation by increasing the expression of mitotic telophase-related genes. Moreover, the drug promoted the adaptive immune response by enhancing the antigen presentation of the major histocompatibility complex II (**Figure 7C**).

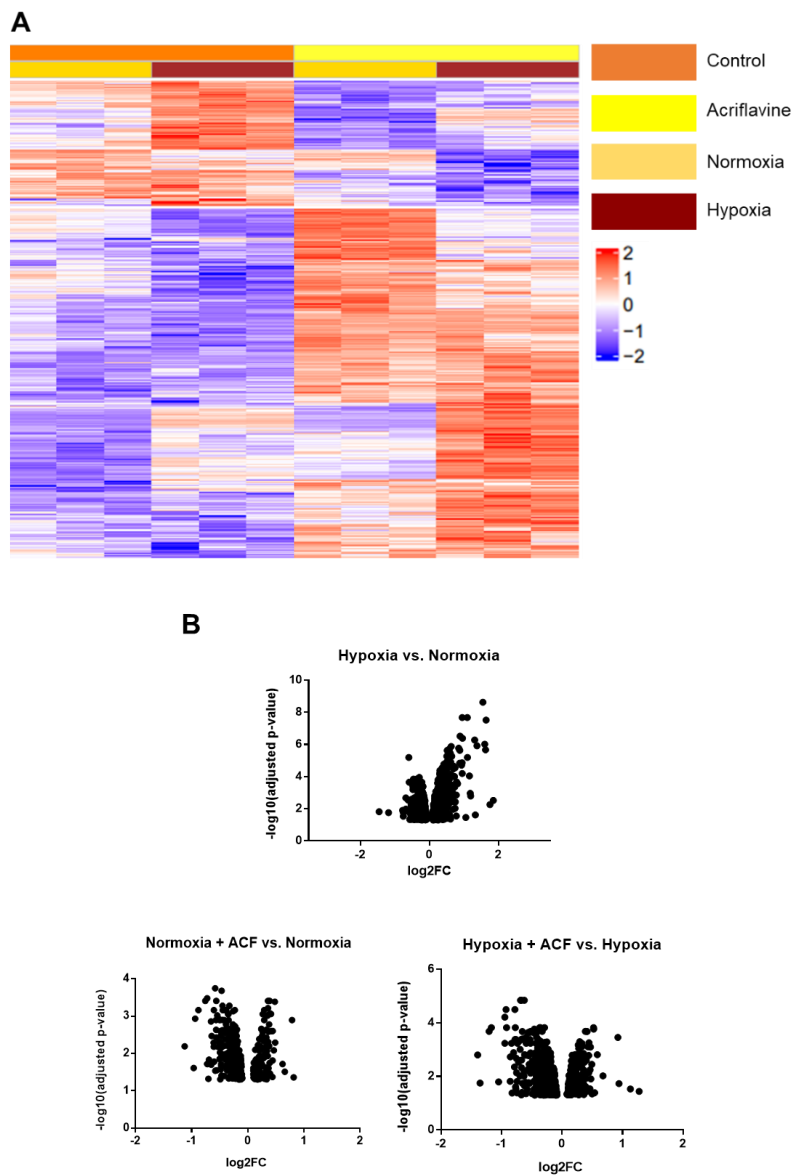


Figure 6. Proteomic analysis of 4T1 cell line. **A:** Heatmap of significant protein alterations in response to hypoxic and acriflavine treatment. Each row represents a protein and each column a sample group. The blue and red colors indicate the expression profile, upregulated or downregulated proteins respectively. **B:** Volcano plot of significant protein alterations in response to hypoxia and to acriflavine treatment under different conditions. Each point represents a protein, with the x-axis showing log₂ fold change and the y-axis displaying -log₁₀(p-value). Multiple testing correction was applied and FDR < 0.05 was considered significant. Heatmaps were plotted using the ComplexHeatmap R package.

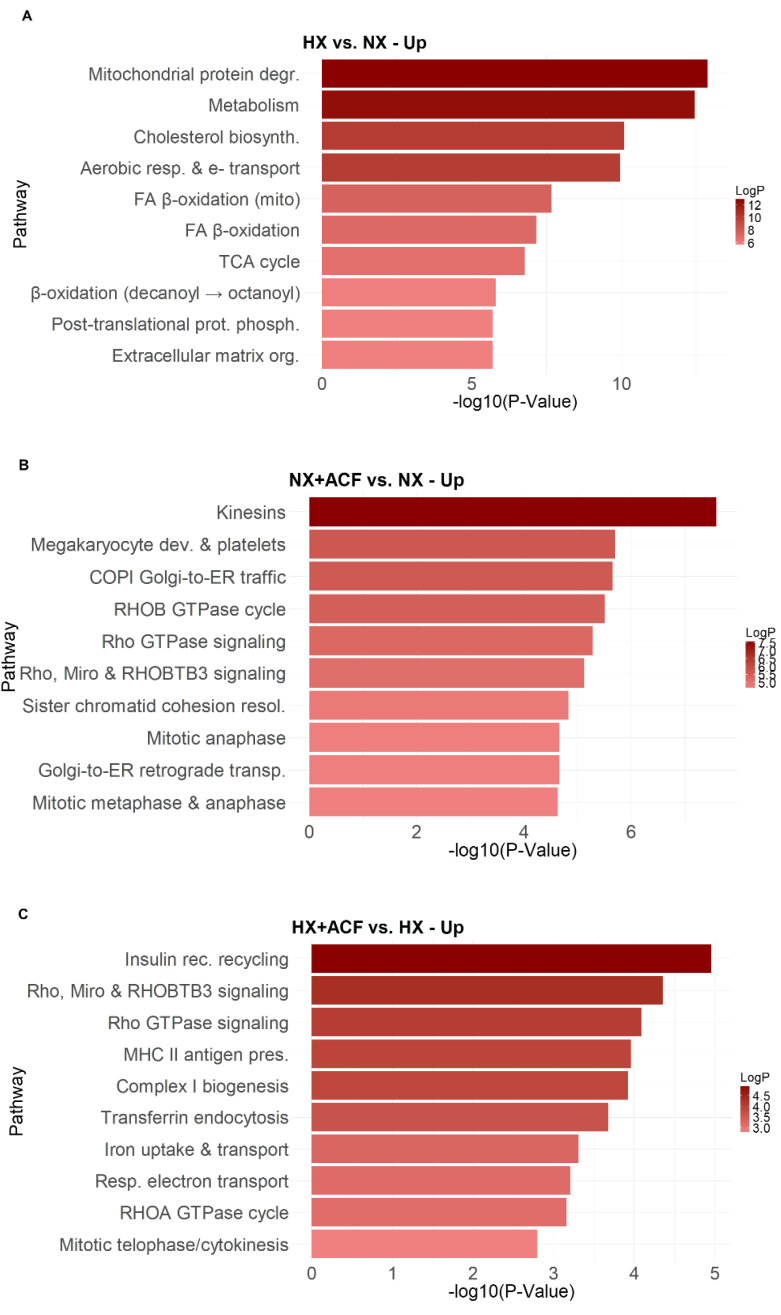


Figure 7. Upregulated Reactome Pathways. The top 10 upregulated Reactome pathways were identified using DAVID Bioinformatics across three comparisons: Hypoxia vs. Normoxia (A), Normoxia+ACF vs. Normoxia (B), and Hypoxia+ACF vs. Hypoxia (C). Bars indicate $-\log_{10}(\text{P-Value})$, with a color gradient reflecting statistical significance. Only pathways meeting the significance threshold (P-adjusted < 0.05) are shown. HX: Hypoxia, NX: Normoxia, A: Acriflavine

Hypoxic treatment downregulated the RNA metabolism and the production and function of ribosomes. Moreover, the ternary complex and 43S formation, and the cap-dependent translation initiation were downregulated too (**Figure 8A**). Acriflavine, under normoxia, suppressed the mitochondrial translation. Moreover, it inhibited RNA and protein metabolism and global translation (**Figure 8B**). The ribosomal activity and the metabolism of proteins and nucleotides were suppressed under hypoxia (**Figure 8C**). Concluding the finding of the proteomic analysis, we claim that hypoxic treatment significantly alters cell metabolism, migratory properties, and proliferation. Acriflavine acts actively under normoxia and hypoxia by interfering with microtubule dynamics, cytoskeletal remodeling, intracellular trafficking, mitotic regulation, and translational activity.

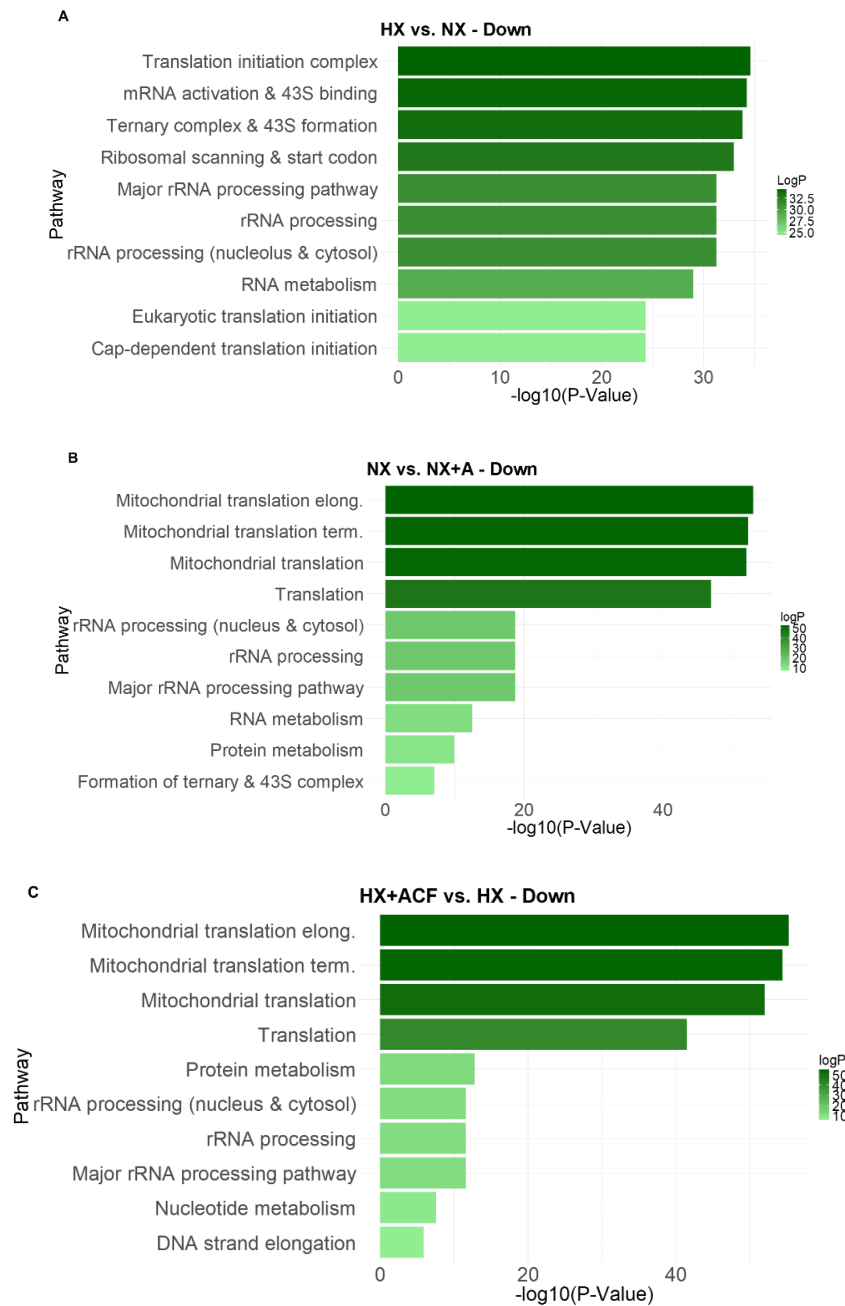


Figure 8. Downregulated Reactome Pathways. The top 10 downregulated Reactome pathways were identified using DAVID Bioinformatics across three comparisons: Hypoxia vs. Normoxia (A), Normoxia+ACF vs. Normoxia (B), and Hypoxia+ACF vs. Hypoxia (C). Bars indicate $-\log_{10}(\text{P-Value})$, with a color gradient reflecting statistical significance. Only pathways meeting the significance threshold (P-adjusted < 0.05) are shown. HX: Hypoxia, NX: Normoxia, A: Acriflavine

4.3. Molecular analysis of *in vitro* hypoxia induction and inhibition

To confirm the findings of proteomic analysis and to evaluate the *in vitro* hypoxia-inducible potential of CoCl₂, and the HIF-1 inhibitory capacity of acriflavine, a TNBC cell line, MDA-MB-231 was treated with the compounds. Thereafter, the underlying protein expression alterations were assessed by the western blot technique. The protein expression alterations in CoCl₂-treated samples were compared to the protein profile of samples undergoing hypoxic incubation. The expression of HIF-1 α was elevated in response to both CoCl₂ treatment and hypoxic incubation. Interestingly, acriflavine treatment reversed this elevation in the CoCl₂-treated group, but not in the hypoxia incubated one. A similar pattern was observed in p-AKT, an important representative of the PI3K pathway, driving cell proliferation. E-cadherin (ECAD), epithelial marker expression was induced by CoCl₂ treatment but not by hypoxic incubation. Acriflavine suppressed the increased ECAD level. In summary, CoCl₂ served as a trustable hypoxia-inducer, while acriflavine proved its HIF-1 inhibitory potential (**Figure 9**).

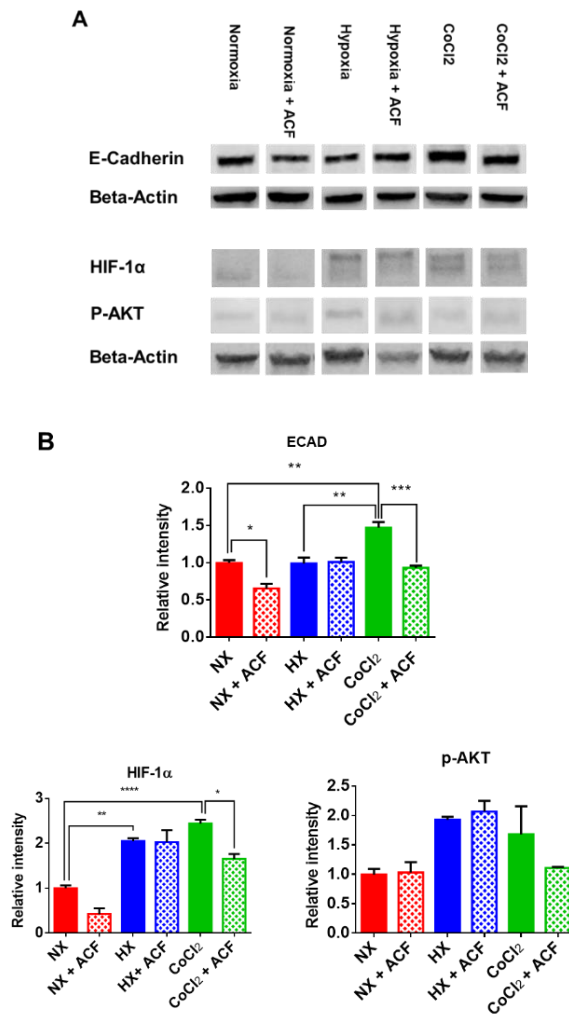


Figure 9. Protein expression analysis in CoCl₂ and acriflavine treated MDA-MB-231 cell line. Cells were either incubated under atmospheric oxygen level or with the application of CoCl₂ hypoxia-mimicking agent. In each condition, 0.5 μM acriflavine was applied. **A:** Representative bands of protein expression levels **B:** Quantitative analysis of ECAD, HIF-1α, and p-AKT protein expressions (N=3, mean + SEM). For statistical analysis, one-way ANOVA and Tukey's multiple comparisons test were applied. * P ≤ 0.05, ** P ≤ 0.01, *** P ≤ 0.001, **** P ≤ 0.0001. NX: Normoxia, NX+ACF: Normoxia+ACF, HX: Hypoxia, HX+ACF: Hypoxia+ ACF. The figure was adapted from the author's original publication (71).

4.4. Interaction assessment of acriflavine and paclitaxel

To overcome the possible limitations related to HIF-1 inhibitory therapy alone, we intended to complement acriflavine with a commonly applied cytostatic agent, paclitaxel. To characterize this drug combination the antiproliferative activity of different concentration pairs were assessed by the SynergyFinder software and classified by synergic, additive and antagonistic interactions. The drug combination was tested on six breast and ovarian cancer cell lines under hypoxic and normoxic conditions. Generally, higher doses of acriflavine simultaneously applied with paclitaxel diminished cell proliferation. In the case of BC cell lines, the additional acriflavine to paclitaxel presented the most notable proliferation inhibitory potential on the two TNBC lines, MDA-MB-231 and HS578T. The drug combination effectively inhibited proliferation of TNBC cells under both conditions. On the contrary, the HER2+ cell line, MDA-MB-453 showed differential response under the different incubation conditions. The complementary acriflavine suppressed the viability more notably on hypoxia. Assessing the type of the drug interactions, we identified additive interaction in the cases of HS578T and MDA-MB-453, and a synergistic interplay on MDA-MB-231. The most synergistic areas on the synergy maps were cell line dependent. Interestingly, under hypoxia the most synergistic regions were identified over 600 nM acriflavine concentration with variable paclitaxel levels. Controversially, under normoxic incubation, the most beneficial concentration pairs were obtained with a lower dose of 200-600 nM acriflavine (**Figure 10A-B**).

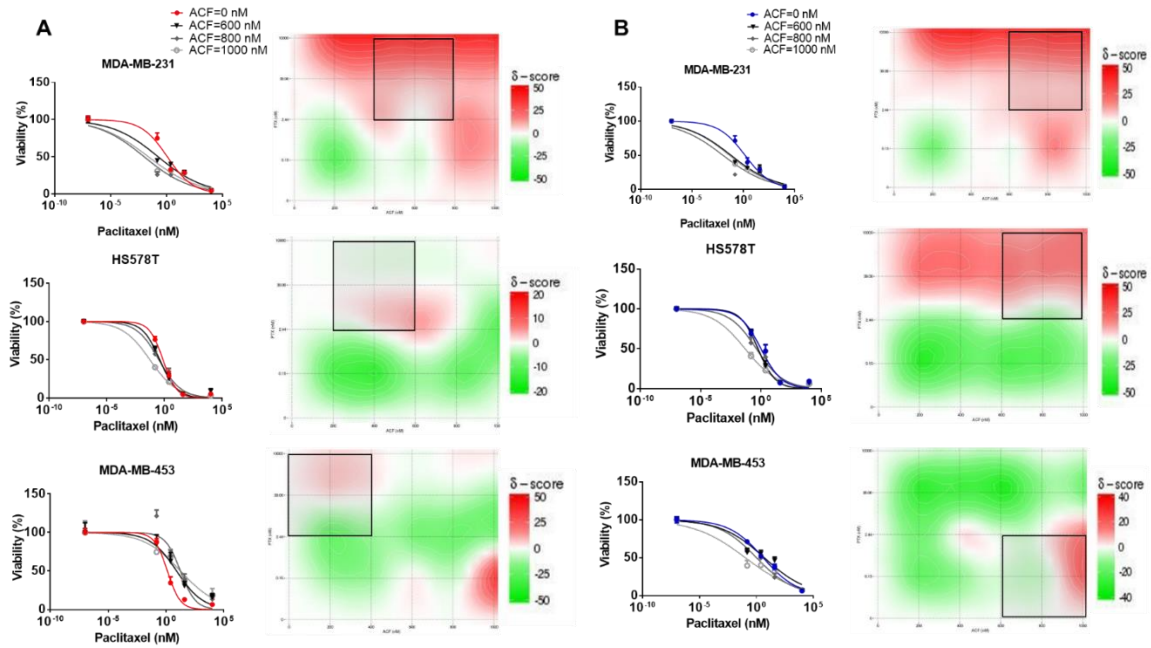


Figure 10: The combined antiproliferative effect of acriflavine and paclitaxel on breast cancer cell lines under normoxic and hypoxic conditions. Different paclitaxel concentrations were combined with different acriflavine concentrations for 72 hours, then the cell viability was assessed by SRB assay. The dose-response curves (N=3, mean + SEM) and the underlying synergy maps are illustrated – MDA-MB-231, HS578T, and MDA-MB-453 cell lines in normoxia (A) and in hypoxia (B). The most synergistic areas are marked with black squares. The figure was adapted from the author’s original publication (71).

The antiproliferative efficacy of the drug combination was remarkable in the case of ovarian cancer cell lines as well. The antiproliferative activity of paclitaxel was enhanced by the increasing dose of acriflavine independently from the incubation condition. The additional 800 nM acriflavine to paclitaxel maximized the proliferation inhibition of SK-OV-3 and OVCAR-8 cells. The most notable shift between normoxia and hypoxia was observed in the case of OVCAR-3 cell line. It showed a gradual antiproliferative efficacy elevation by the increasing acriflavine concentration under normoxia. However, in response to the hypoxic treatment, the lowest dose of acriflavine evoked an identical effect compared to the highest dose of the drug. Regarding the OVCAR-3 cell line, SynergyFinder software marked an antagonistic interaction. Acriflavine and paclitaxel strengthened the mutual effect by additive interaction in SK-OV-3 and OVCAR-8 cells (**Figure 11**).

To conclude, the drug combination was proved to be efficient in proliferation inhibition in each cell line. In the majority of the cases, we identified additive interactions, and the most favorable outcome, a synergistic interplay of acriflavine and paclitaxel was observed in the case of the MDA-MB-231 TNBC cell line.

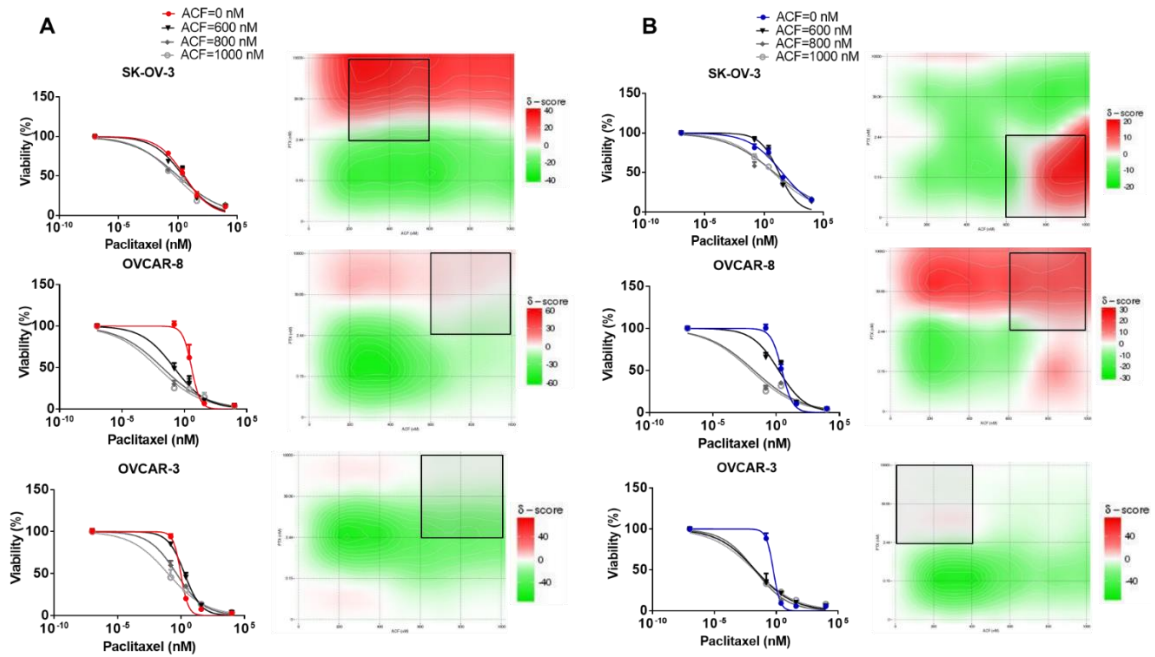


Figure 11: The combined antiproliferative effect of acriflavine and paclitaxel on ovarian cancer cell lines under normoxic and hypoxic conditions. Different paclitaxel concentrations were combined with different acriflavine concentrations for 72 hours, then the cell viability was assessed by SRB assay. The dose-response curves (N=3, mean + SEM) and the underlying synergy maps are illustrated – SK-OV-3, OVCAR-8, and OVCAR-3 cell lines in normoxia (A) and in hypoxia (B). The most synergistic areas are marked with black squares. The figure was adapted from the author’s original publication (71).

4.5. Migratory assessment of the combination treatment

Considering the promising results of the antiproliferative efficacy we continued with studying the anti-migratory effect of the drug combination. To further increase the migration inhibitory potential we involved an EMT inhibitory compound, rolipram as well. Wound-healing assay was conducted under normoxic and hypoxic conditions and the wound-closing inhibitory potential of the mono- and combination treatments was assessed. The migration was inhibited by the monotherapies under both conditions, with a more notable impact under hypoxia. The ACF+PTX combination therapy treatment resulted in significant migration inhibition in normoxia. The additional rolipram slightly increased this effect. However, under hypoxia, the complementary rolipram remarkably decreased the migration compared to ACF and PTX mono- and combinatory therapies. Consequently, the ACF+PTX efficiently inhibited migration under both conditions, with a more prominent effect under hypoxia with supplementary rolipram (**Figure 12A-B**).

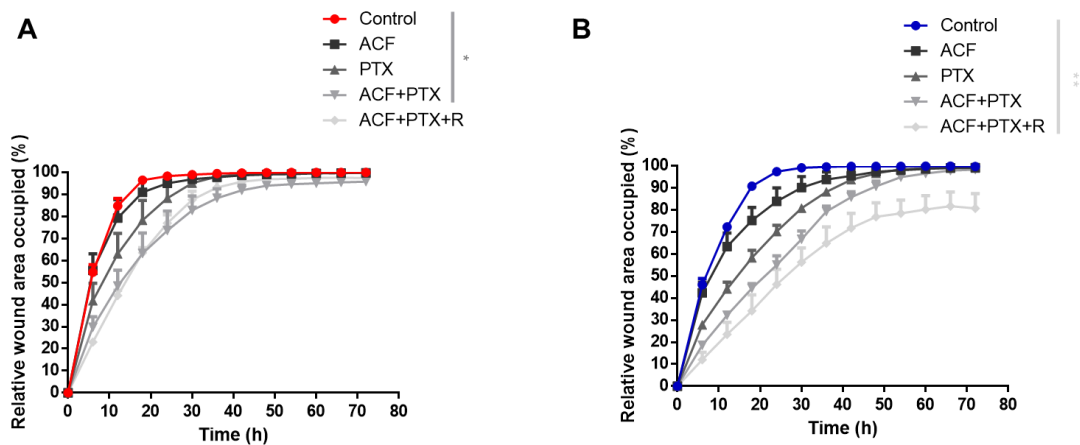


Figure 12. 72-hour-long wound healing assay of MDA-MB-231 cells under normoxia (A) and hypoxia (B). The cells were treated with either acriflavine (ACF) or paclitaxel (PTX) in mono- and combination therapy with an additional epithelial-mesenchymal transition inhibitor rolipram (R), then wound healing ability was assessed. For statistical analysis, Kruskal-Wallis and Dunn's multiple comparison tests were used (N=3, mean + SEM). *P ≤ 0.05, ** P ≤ 0.01. The figure was adapted from the author's original publication (71).

4.6. Assessment of the *in vivo* hypoxia-inducible impact of CoCl₂

To assess the HIF-1 stabilizing property of the prolyl hydroxylase inhibitor, CoCl₂ mice were subjected to CoCl₂ treatment via different administration routes. After 21 days, the mice were terminated and the mRNA expression of NDRG1 – a key HIF-1 target gene – was quantified by qPCR in the dissected kidneys. Each CoCl₂-treated group showed an elevated NDRG1 mRNA expression compared to the control confirming its HIF-1 inducible property. The most prominent NDRG1 accumulation occurred in the group that received the compound ad libitum mixed with drinking water. Considering the good tolerability of CoCl₂ application in drinking water, for *in vivo* hypoxia modeling we opted for administering CoCl₂ in drinking water (**Figure 13**).

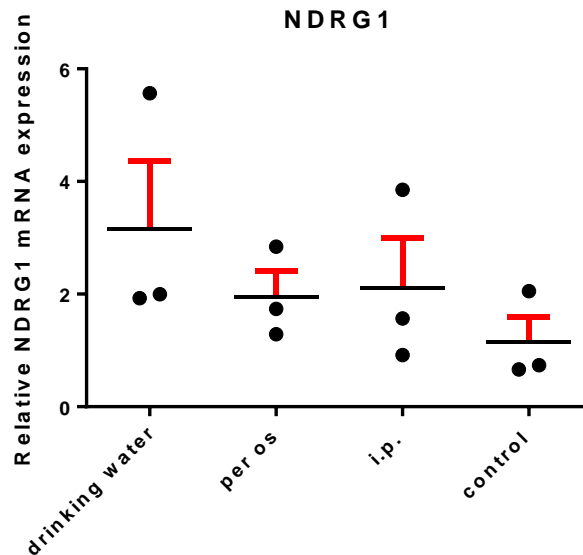


Figure 13. NDRG1 mRNA expression in mice kidneys upon CoCl₂ treatment applied via different administration routes over 21 days (ad libitum access by mixing CoCl₂ solution with drinking water (260 mg/l), per os application by using an oral gavage (40 mg/kg) or by intraperitoneal injection (40 mg/kg) three times per week.

4.7. *In vivo* safety and efficacy evaluation of the drug combination

Following the *in vitro* assays and the *in vivo* hypoxia-inducible potential assessment of CoCl₂, we evaluated the drug combination's *in vivo* safety and efficacy. First, toxicity analysis was conducted based on body weight, liver-body weight ratio, and liver histology assessments. We did not observe any alterations in the body weight and the liver body weight ratio in response to the mono- or combination therapies (**Figure 14A-B**). Moreover, the morphology of the liver tissue sections was comparable with the control, hence we concluded that the application of the drugs either in mono- or combination therapy is tolerable (**Figure 14C**).

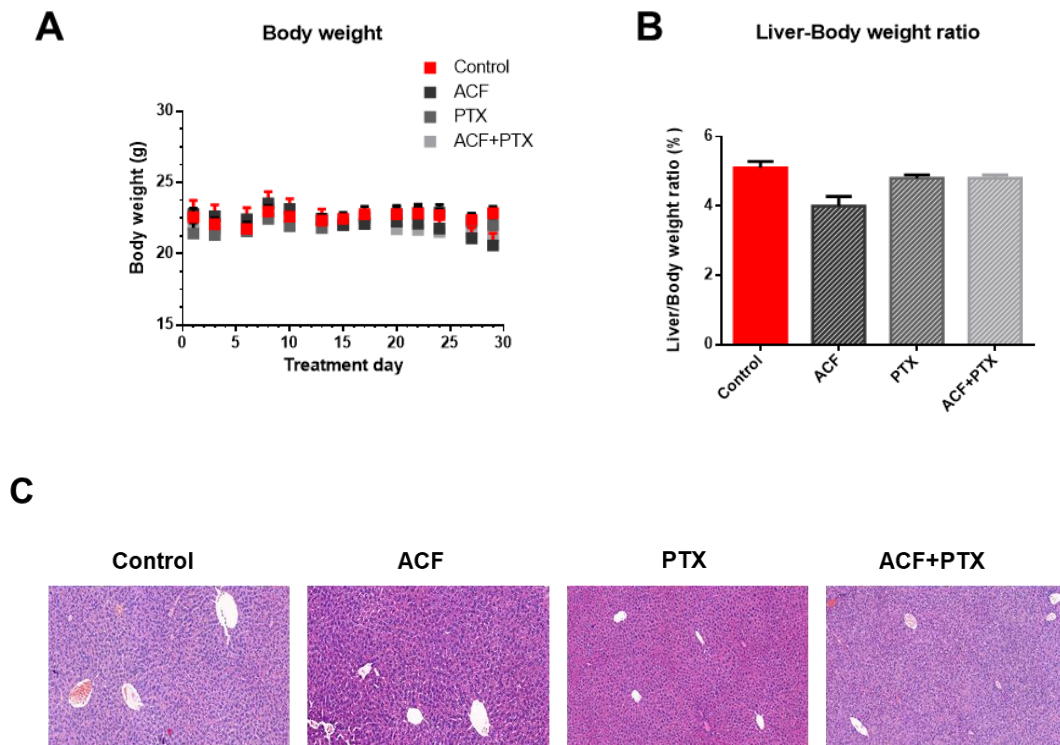


Figure 14. Safety assessment of acriflavine and paclitaxel mono- and combination. **A:** Body weight shift during the treatment period (N=7, mean + SEM), **B:** Liver/Body weight ratios, **C:** Liver tissue sections. The figure was adapted from the author's original publication (71).

The *in vivo* tumor-inhibitory potential of the drug combination was studied on orthotopic breast MDA-MB-231 xenografts. The tumor growth and macrometastasis development were compared to untreated, ACF and PTX monotherapy-treated groups. The efficacy was assessed with and without hypoxia-mimicking. Interestingly, without CoCl_2 the application of acriflavine monotherapy significantly reduced the tumor growth. The combination therapy efficiently suppressed the tumor development both with and without CoCl_2 (**Figure 15A-B**). Macrometastasis formation was inhibited in each ACF and PTX-treated group, except in ACF monotherapy with CoCl_2 (**Figure 15C**).

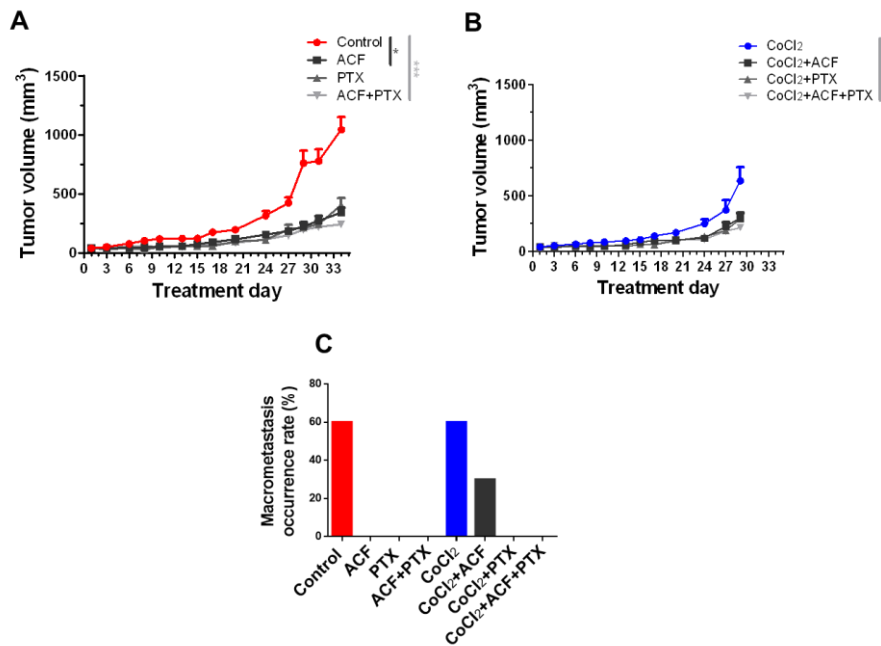


Figure 15. Efficacy assessment of acriflavine and paclitaxel mono- and combination therapy by using MDA-MB-231 orthotopic breast xenograft model. 200 mg/liter CoCl_2 was applied in the drinking water to model *in vivo* hypoxia. Acriflavine and paclitaxel were applied intraperitoneally in 8 mg/kg and 5 mg/kg doses respectively three times per week. Tumor volume shift in response to the treatment without (**A**) and with CoCl_2 (**B**) application (N=7, mean + SEM). **C**: Macrometastasis occurrence rate at post-mortem macrometastasis (>2 mm) detection. For statistical analysis, the Kruskal-Wallis test was applied. * $P \leq 0.05$, ** $P \leq 0.01$, *** $P \leq 0.001$. The figure was adapted from the author's original publication (71).

4.8. Molecular analysis of the orthotopic xenografts

The orthotopic MDA-MB-231 xenografts were subjected to molecular analysis. Protein expression alterations of ECAD, HIF-1 α , and p-AKT were studied by western blot technique. The ECAD expression was suppressed by CoCl₂ application compared to the control group, while additional ACF and ACF+PTX treatments increased the ECAD level. The ECAD alterations were more moderate without hypoxia-mimicking. HIF-1 α expression was promoted by CoCl₂ application in the tumor tissue, however only the ACF+PTX combination therapy was efficient in mitigating this elevation. An important representative of the PI3K cell signaling pathway, p-AKT was enhanced by CoCl₂ treatment. The simultaneous application of ACF and PTX notably suppressed p-AKT levels (**Figure 16**).

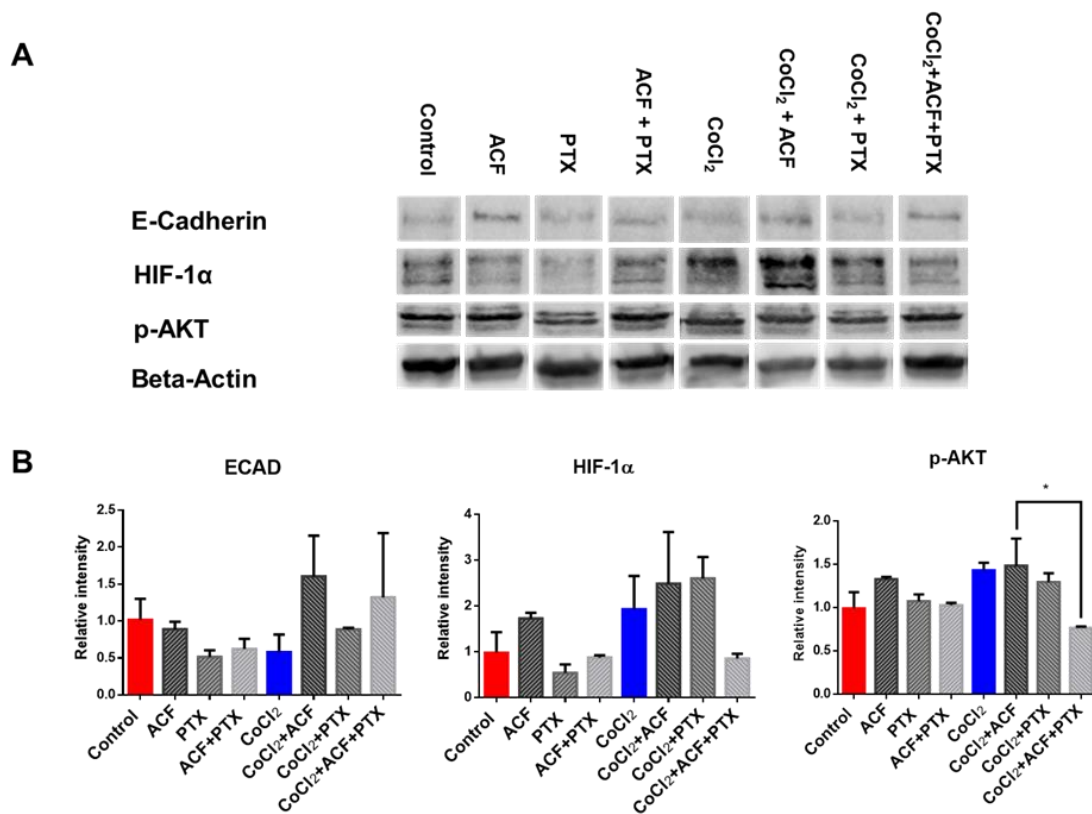


Figure 16. Protein expression of important representatives of proliferation and related metastasis-related signaling pathways and of ECAD in MDA-MB-231 xenografts treated with either ACF or PTX or their combination. 200 mg/liter CoCl₂ was used as a hypoxia-inducer. **A:** Schematic representation of the protein expression signals (ECAD, HIF-1α, p-AKT). Beta-actin was used as reference gene. **B:** Densitometric analysis of the protein expressions in response to ACF and PTX mono- or combination treatment with and without CoCl₂ treatment. The samples were normalized on the expression of the housekeeping gene, Beta-Actin (N=3, mean + SEM). For statistical analysis, one-way ANOVA and Tukey's multiple comparisons test were used. * P ≤ 0.05. The figure was adapted from the author's original publication (71).

4.9. HIF-1 α and PD-L1 co-expression assessment

Considering the successful application of the HIF-1 inhibitory therapy alone and in combination with paclitaxel, we were eager to assess the rationale behind combining HIF-1 inhibitors with ICIs. Hence, as a primary step, we carried out *in silico* studies to evaluate the correlation of HIF-1 α and PD-L1 by using the TCGA Breast database. We observed a positive correlation between the mRNA expression of HIF-1 α and PD-L1. The increasing HIF-1 α levels proportionally correlated with higher PD-L1 expression (**Figure 17**).

Then, HIF-1 α and PD-L1 protein expressions were analyzed using the TMAs of different subtypes of breast tumors originating from treatment-naive patients. We identified a positive correlation between the two proteins (**Figure 18**). The positive slopes of both mRNA and protein levels indicate a positive relationship, however, the low R^2 values (0.12 and 0.084) suggest that this relationship is weak due to the high variability among clinical samples (**Figure 17-18**). Considering the positive correlation between HIF-1 α and PD-L1 in clinical samples, we are eager to develop suitable preclinical models to test the simultaneous efficacy of the inhibitors.

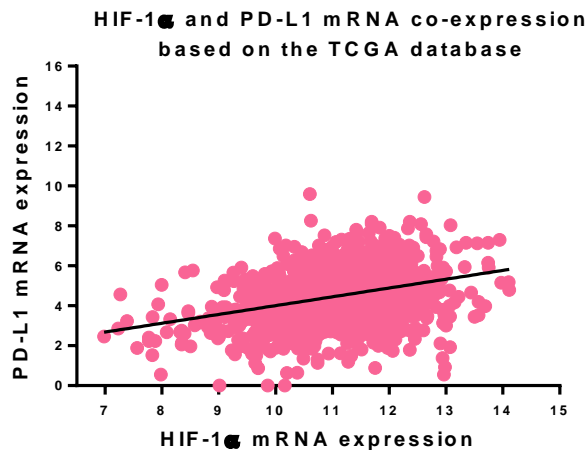


Figure 17. The mRNA expression correlation between HIF-1 α and PD-L1 in breast cancer ($R^2=0.12$). The data was derived from the TCGA breast database. The data presented on the scatter plot originates from the University of California, Xena platform based on The Cancer Genome Atlas (TCGA) Breast Cancer Database and gene expression datasets (45).

HIF-1 α and PD-L1 protein co-expression in clinical breast tumor samples

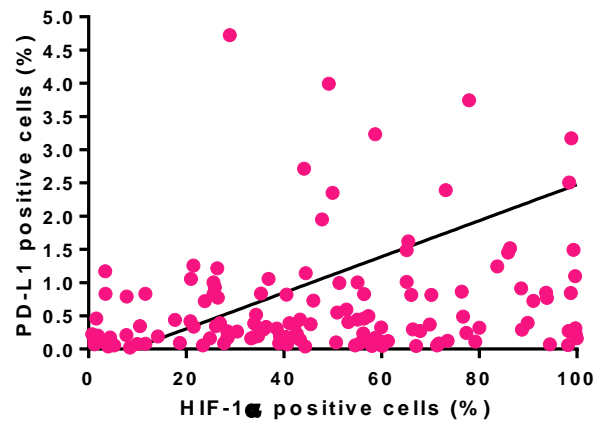


Figure 18. The protein expression correlation between HIF-1 α and PD-L1 in clinical breast tumor samples ($R^2=0.084$). The protein expression was assessed by the immunohistochemical method using tumor microarrays of freshly diagnosed, non-metastasized treatment-naïve breast tumors originating from female patients aged 30-90 years.

5. Discussion

Tumor hypoxia is a common feature of breast and ovarian tumors. It is one of the major contributors to tumor progression by significantly enhancing metastasis development (35). Therefore, inhibiting the hypoxia network is an essential therapeutic approach. Even though the successful preclinical results, most HIF-1 inhibitors failed in clinical trials when applied in monotherapies (54). Promising results appeared upon combining HIF-1 inhibitors with conventional chemotherapeutic agents, kinase inhibitors, and other targeted therapies (56). We intended to extend the therapeutic options for breast and ovarian cancers by novel combination strategies. Therefore, in our studies, we selected a clinically not yet tested dual HIF-1, HIF-2 inhibitor, acriflavine, and as a complementary treatment we opted for a widely used taxane, paclitaxel. Moreover, the rationale behind the simultaneous application of HIF-1 inhibitors and ICIs in breast cancer treatment was also evaluated.

First, the antiproliferative efficacy of acriflavine was analyzed on seven different breast and ovarian cancer cell lines. Acriflavine effectively inhibited the proliferation of breast and ovarian cancer cells which finding was consistent with other's results. For instance, Lee et al. observed a notable proliferation suppressive impact of ACF on MDA-MB-231 and HS578T cells (72). Hassan et al. pointed out the remarkably high cell viability reducing the potential of ACF compared to the clinically used compounds, 5-fluorouracil or irinotecan (73). Interestingly, in most cases, the proliferation inhibitory potential of acriflavine was higher under normoxia, than in hypoxia. HIF-1 is a well-known modulator of drug efflux pumps, contributing to resistance (74). Consequently, as some representatives of ATP-binding cassette (ABC) transporters are HIF-1 target genes (75), we hypothesize that the chronic hypoxic treatment enhanced drug efflux by the activation of those. The highest selectivity ratios between normoxia and hypoxia were observed in the case of the human TNBC cell lines, MDA-MB-231 and HS578T, indicating the lack of sensitivity for hypoxic conditions. To ensure the possibility of assessing the *in vivo* anti-tumor effect of ACF in the context of an intact immune system, we also evaluated its antiproliferative efficacy on the 4T1 cell line, a suitable allograft model. ACF also effectively inhibited the proliferation of the 4T1, murine TNBC cells.

To investigate the mechanism of action of ACF and the hypoxia treatment-induced alterations in the proteomic profile, we conducted proteomic analysis on the 4T1 cells. The hypoxic treatment significantly altered the proteomic profile by inducing the expression of numerous proteins. In parallel, a smaller group of proteins were downregulated. Evaluating the shifts that occurred in the protein expressions by acriflavine treatment, we conclude that ACF mostly functioned as a down regulator. Conversely, a lower number of proteins exhibited upregulation upon ACF treatment.

Up-and-downregulated pathway analysis was conducted using the DAVID tool. Importantly, when analyzing pathway alterations, we refer to a wide range of regulator genes involved in specific processes. Hypoxic treatment caused upregulation in pathways involved in metabolic processes and ECM remodeling. On the contrary, it downregulated key pathways involved in global translation, suggesting the metabolic switch to an exclusive translation of essential proteins. The acriflavine-altered pathways showed a similar pattern under hypoxic conditions. The drug upregulated pathways of Rho GTPase signaling, mitosis, and metabolism of essential molecules, suggesting interference with migration, cell proliferation, and cellular metabolism. It inhibited RNA and protein metabolism and global translation. Furthermore, ACF suppressed the mitochondrial translation leading to reduced oxidative phosphorylation. Consequently, ACF acts by affecting microtubule dynamics, cytoskeletal remodeling, intracellular trafficking, mitotic regulation, and translational activity. Research groups of Fan and Martí Díaz previously stated that acriflavine induces apoptosis, and autophagy and interferes with glucose metabolism (51,76). Our results align with the already existing findings, moreover, these notably expanded the current knowledge regarding the mechanism of action of ACF.

We confirmed the findings of the proteomic profiling by assessing the protein expression of HIF-1 α , ECAD, and p-AKT by western blot. Moreover, we aimed to verify the hypoxia-inducible potential of CoCl₂ stated by Ho Pak et al (77). The elevated expression of HIF-1 α in response to CoCl₂ treatment and hypoxic incubation confirmed the applicability of CoCl₂ as *in vitro* hypoxia inducer. Interestingly, the impact of ACF was more remarkable in the CoCl₂-treated groups compared to the hypoxia-treated ones. Acriflavine suppressed the expression of HIF-1 α and p-AKT, confirming its potential to block the hypoxia cascade and inhibit cell proliferation. ACF reverted the elevation in

ECAD upon CoCl_2 treatment. This finding suggests that ACF bears EMT-regulating potential (78). The EMT-inhibitory potential of ACF was described in pancreatic cancer model (79), however not yet been evaluated in breast cancer.

Following the evaluation of acriflavine in monotherapy, we studied its inhibitory potential on the proliferation of breast and ovarian cancer cells together with paclitaxel. The assessment of the simultaneous antiproliferative efficacy of ACF and PTX indicated that the higher doses of complementary acriflavine increase the toxic potential of paclitaxel. Furthermore, the drug interaction analysis exhibited additive interactions in the vast majority of the cell lines, moreover a synergistic interplay was also identified. A comprehensive review pointed out the successful application of combining HIF-1 inhibitors and other therapeutic agents (56). Our finding agrees with these results, however, the ACF and PTX combination against breast and ovarian cancer has not yet been reported by others. Lipid nanoparticle encapsulated ACF and PTX were tested in combination against colorectal cancer-associated fibroblasts, however, synergistic interaction was not detected in this model (80).

The alterations that occurred in the proteomic profile of TNBC cells indicated that acriflavine affects the migratory potential of the cells. Therefore, a functional migratory test, wound-healing assay was conducted to analyze the anti-migratory potential of the drug combination. To further increase the migration inhibitory potential, the drug combination was complemented with rolipram, an EMT inhibitory compound (81). Moreover, we were eager to test whether the hypoxic incubation enhances motility as stated elsewhere (82). Unexpectedly, the hypoxic treatment reduced the wound healing velocity. Paclitaxel alone exerted a minimal migration-suppressing ability, however, the complementary acriflavine notably increased its efficacy. Paclitaxel alone was described as a less potent migration inhibitory compound in other studies too (83). The dual drug combination of acriflavine and paclitaxel significantly decreased the motility of MD-MB-231 TNBC cells under normoxia. Generally, the long-term hypoxic treatment slightly reduced the motility of the cells. The inhibitory effect of the drugs on migration was even more pronounced under hypoxic conditions, particularly with the addition of rolipram. Considering the phosphodiesterase activity of rolipram, this can be explained by the increased intracellular cAMP levels inhibiting HIF-1 α signaling, alongside the HIF-1 dimerization inhibitory effect of ACF. Importantly, the cells were exposed to a 72-hour-

long hypoxic treatment, pointing out the possibility of the activation of compensatory mechanisms. Therefore, in future studies we plan to introduce intermittent hypoxic treatment (84), modeling a more realistic picture of the hypoxic tumor environment.

After completing the deep investigation on *in vitro* systems, we intended to test the drug's safety and anti-cancer efficacy in xenograft models. To ensure the opportunity to investigate the efficacy of the compounds in the presence of a hypoxic tumor microenvironment, a proper *in vivo* hypoxia model establishment was necessary. An earlier study suggested the application of CoCl₂ as *in vivo* hypoxia inducer (85). Therefore, the hypoxia-mimicking effect of CoCl₂ was studied by testing different administration routes of CoCl₂ application. The hypoxia-inducible potency was assessed by measuring the mRNA expression of a HIF-1 target gene, NDRG1 in kidneys. The most remarkable NDRG1 elevation was observed when CoCl₂ was mixed with drinking water. Therefore, in later studies, we opted for this technique to model hypoxia *in vivo*.

The *in vivo* anti-tumor efficacy of ACF and the ACF+PTX drug combination was evaluated using an MDA-MB-231 orthotopic breast xenograft model. The efficacy study was conducted with and without hypoxia stimulation. The drug combination effectively inhibited tumor growth and macrometastasis formation independently from the oxygenation of the tissues. Consequently, we identified a safe and efficient combination therapeutic strategy against TNBC. This novel approach was not yet tested on *in vivo* systems by others, suggesting that further *ex vivo* studies were needed to validate its efficacy.

The MDA-MB-231 xenografts, originating from the mammary fat pad of the mice were processed and then subjected to protein expression analysis by western blotting. Our results indicated that the combination therapy effectively diminished HIF-1 α and p-AKT levels and increased ECAD. Accordingly, the activation of the hypoxia cascade, the migration, and the cell growth and survival were suppressed. Additionally, Kashiwagi et al. claim that ECAD could serve as a prognostic marker of TNBC (86), therefore the EMT decreasing potency might lead to improved outcomes.

Given the promising results observed with the application of a HIF-1 inhibitory drug in combination with other therapies, we aimed to explore the clinical rationale behind the simultaneous use of ICIs and HIF-1 inhibitors in breast cancer treatment. HIF-1 and PD-

L1 have a direct correlation with PD-L1 having HRE on the promoter (60). Therefore, the mRNA co-expression of HIF-1 α and PD-L1 was studied in in-silico systems. The results were validated by evaluating the expressions on the protein level. We observed a relationship between the two genes, suggesting the possibility of dual inhibition. Currently, only a limited number of preclinical and clinical studies have been introduced that investigated the mutual efficacy of HIF-1 inhibitors and ICIs (87–89). Therefore, we plan to establish further preclinical models to study these drug combinations in a broad range of cancer types where immunotherapy is applied.

6. Conclusion

In this study, we investigated the effects of tumor hypoxia on cell growth, proliferation, survival, migration, and immune functions in preclinical systems, and clinical samples. Furthermore, we also studied the possibilities of targeting tumor hypoxia and its underlying cascade to prevent tumor progression by focusing on the clinically not yet tested HIF-1/2 inhibitory compound, acriflavine. Mono- and combined therapeutic approaches with paclitaxel were simultaneously investigated.

Our results indicate the following findings and achievements:

(1) An *in vitro* hypoxia modeling system, suitable for studying the mutual drug effects and drug interactions, was established. Tumor hypoxia significantly altered the proliferation, metabolism, transcription, and translation processes in TNBC cells by upregulating and downregulating key regulatory pathways.

(2) A synergistic drug combination, acriflavine and paclitaxel effectively inhibited the proliferation of MDA-MB-231 cells, the growth of cell line-derived xenografts, and the formation of macrometastases. Additionally, the drug combination presented an additive effect in the vast majority of the tested breast and ovarian cancer cell lines. Acriflavine and the drug combination did not cause any side effects in mice, proving their safe application.

(3) Acriflavine modulated the protein expression of multiple pathways involved in cell growth, metabolic processes, gene expression, protein synthesis, and immune function, effectively counteracting hypoxia-induced effects. The drug specifically influenced p-AKT and HIF-1 α levels and exhibited a notable effect even under normoxic conditions as well.

(4) Acriflavine inhibited EMT, by increasing ECAD protein expression of MDA-MB-231 xenografts and modulating the Rho GTPase signaling of 4T1 TNBC cells. The administration of an additional, EMT inhibitory compound, rolipram with the acriflavine and paclitaxel drug combination remarkably suppressed the migration of TNBC cells under hypoxia.

(5) We found the rationale behind combining HIF-1 inhibitors and ICIs in breast cancer treatment.

In summary, our results suggest that the hypoxia-cascade can be reversed. The novel therapeutic approaches studied in this research offer effective solutions by demonstrating the potential to suppress metastasis formation, thereby increasing survival.

7. Summary

Tumor hypoxia is a common feature of solid tumors and it significantly contributes to tumor progression by enhancing metastasis development. The underlying processes of tumor hypoxia are driven by the hypoxia-inducible factor 1 (HIF-1). By being responsible for the transcription of numerous genes involved in tumor progression, HIF-1 is an attractive drug target. However, HIF-1 inhibitory drugs applied as monotherapies failed in clinical trials. The combination of HIF-1 inhibitors with other therapeutics increased the efficacy of the treatment regimens. In our study, we aimed to explore strategies to improve these essential therapeutics for the treatment of highly metastasizing breast and ovarian cancers. Following suitable *in vitro* and *in vivo* hypoxia model establishments, the research was driven by complex drug-drug interaction studies, molecular and functional assays, *in vivo* safety and efficacy studies, proteomic and database examinations. Based on the promising preclinical background, as a HIF-1 inhibitory compound, we selected acriflavine. The antiproliferative activity of the drug was proved on a panel of breast and ovarian cancer cell lines, with the highest efficacy on triple-negative breast cancer cell lines. The proteomic profiling of these cells suggests that acriflavine interferes with migration, cell proliferation, and cellular metabolism. We opted for involving complementary treatment alongside evaluating HIF-1 inhibitory therapy. Therefore, a commonly applied taxane in breast and ovarian cancer treatment, paclitaxel was used in parallel with acriflavine. Additionally, recognizing the significance of epithelial-mesenchymal transition (EMT) in metastasis formation, an EMT-targeting compound was also analyzed. We identified a synergistic drug combination of acriflavine and paclitaxel that significantly suppressed tumor growth and metastasis formation. Enhancing this dual therapy with the EMT-inhibitory agent rolipram further strengthened its anti-metastatic effects. Based on the promising results of combining HIF-1 inhibitors with other therapies we were encouraged to evaluate the rationale behind combining ICIs and HIF-1 inhibitors. Our findings provide a clinical rationale for the concurrent use of HIF-1 inhibitors and immune checkpoint inhibitors in breast cancer treatment. These novel therapeutic strategies offer innovative approaches to tackle highly metastasizing breast and ovarian cancers.

8. References

1. Bray F, Laversanne M, Sung H, Ferlay J, Siegel RL, Soerjomataram I, et al. Global cancer statistics 2022: GLOBOCAN estimates of incidence and mortality worldwide for 36 cancers in 185 countries. *CA Cancer J Clin.* 2024;74(3):229–63.
2. Wang J, Wu SG. Breast Cancer: An Overview of Current Therapeutic Strategies, Challenge, and Perspectives. *Breast Cancer Targets Ther.* 2023;Volume 15:721–30.
3. Kenessey I, Nagy P, Polgár C. The Hungarian situation of cancer epidemiology in the second decade of the 21st century. *Magy Onkol.* 2022;66(3):175–84.
4. Global Cancer Observatory. Cancer Today [Internet]. 2025 [updated 2024 Febr 8; cited 2025 Febr 5]. Available from: <https://gco.iarc.fr/en>
5. Zhou Z, Li M. Targeted therapies for cancer. *BMC Med.* 2022;20(1):90, s12916-022-02287–3.
6. Barot S, Patel H, Yadav A, Ban I. Recent advancement in targeted therapy and role of emerging technologies to treat cancer. *Med Oncol.* 2023;40(11):324.
7. Agostinetti E, Curigliano G, Piccart M. Emerging treatments in HER2-positive advanced breast cancer: Keep raising the bar. *Cell Rep Med.* 2024;5(6):101575.
8. González-Hurtado D, Rivero S, Samamé Pérez-Vargas JC, Petracchi FE. Hormone Receptor-Positive / HER2-Negative Early Breast Cancer High-Risk Population: An Algorithm for Optimization Systemic Adjuvant Treatment Based on 2022 Updates. *Breast Cancer Basic Clin Res.* 2023;17:11782234231192780.
9. Cejuela M, Gil-Torralvo A, Castilla MÁ, Domínguez-Cejudo MÁ, Falcón A, Benavent M, et al. Abemaciclib, Palbociclib, and Ribociclib in Real-World Data: A Direct Comparison of First-Line Treatment for Endocrine-Receptor-Positive Metastatic Breast Cancer. *Int J Mol Sci.* 2023;24(10):8488.

10. Nagpal D, Verma R, Mittal V, Jeandet P, Kaushik D. Targeted therapies against breast cancer: Clinical perspectives, obstacles and new opportunities. *J Drug Deliv Sci Technol.* 2023;89:105049.
11. Papalexis P, Georgakopoulou V, Drossos P, Thymara E, Nonni A, Lazaris A, et al. Precision medicine in breast cancer (Review). *Mol Clin Oncol.* 2024;21(5):78.
12. Liu B, Zhou H, Tan L, Siu KTH, Guan XY. Exploring treatment options in cancer: tumor treatment strategies. *Signal Transduct Target Ther.* 2024;9(1):175.
13. Tavares V, Marques IS, Melo IG de, Assis J, Pereira D, Medeiros R. Paradigm Shift: A Comprehensive Review of Ovarian Cancer Management in an Era of Advancements. *Int J Mol Sci.* 2024;25(3):1845.
14. Mao CL, Seow KM, Chen KH. The Utilization of Bevacizumab in Patients with Advanced Ovarian Cancer: A Systematic Review of the Mechanisms and Effects. *Int J Mol Sci.* 2022;23(13):6911.
15. Koutras AK, Fountzilas G, Makatsoris T, Peroukides S, Kalofonos HP. Bevacizumab in the treatment of breast cancer. *Cancer Treat Rev.* 2010 Feb;36(1):75–82.
16. Heater NK, Warrior S, Lu J. Current and future immunotherapy for breast cancer. *J Hematol Oncol J Hematol Oncol.* 2024;17(1):131.
17. Connor AE, Lyons PM, Kilgallon AM, Simpson JC, Perry AS, Lysaght J. Examining the evidence for immune checkpoint therapy in high-grade serous ovarian cancer. *Heliyon.* 2024;10(20):e38888.
18. Gerstberger S, Jiang Q, Ganesh K. Metastasis. *Cell.* 2023;186(8):1564–79.
19. Tímár J, Csuka O, Orosz Z, Jeney A, Kopper L. Molecular pathology of tumor metastasis. I. Predictive pathology. *Pathol Oncol Res POR.* 2001;7(3):217–30.
20. Tímár J, Csuka O, Orosz Z, Jeney A, Kopper L. Molecular pathology of tumor metastasis: II. Molecular staging and differential diagnosis. *Pathol Oncol Res.* 2002;8(3):204–19.

21. Tímár J, Ladányi A, Peták I, Jeney A, Kopper L. Molecular pathology of tumor metastasis III: Target array and combinatorial therapies. *Pathol Oncol Res.* 2003;9(1):49–72.
22. Fares J, Fares MY, Khachfe HH, Salhab HA, Fares Y. Molecular principles of metastasis: a hallmark of cancer revisited. *Signal Transduct Target Ther.* 2020;5(1):28.
23. Grote I, Poppe A, Lehmann U, Christgen M, Kreipe H, Bartels S. Frequency of genetic alterations differs in advanced breast cancer between metastatic sites. *Genes Chromosomes Cancer.* 2024;63(1):e23199.
24. Deng K, Yang C, Tan Q, Song W, Lu M, Zhao W, et al. Sites of distant metastases and overall survival in ovarian cancer: A study of 1481 patients. *Gynecol Oncol.* 2018;150(3):460–5.
25. Boire A, Burke K, Cox TR, Guise T, Jamal-Hanjani M, Janowitz T, et al. Why do patients with cancer die? *Nat Rev Cancer.* 2024;24(8):578–89.
26. Quintero-Fabián S, Arreola R, Becerril-Villanueva E, Torres-Romero JC, Arana-Argáez V, Lara-Riegos J, et al. Role of Matrix Metalloproteinases in Angiogenesis and Cancer. *Front Oncol.* 2019;9:1370.
27. Bejarano L, Jordão MJC, Joyce JA. Therapeutic Targeting of the Tumor Microenvironment. *Cancer Discov.* 2021;11(4):933–59.
28. Glaviano A, Lau HSH, Carter LM, Lee EHC, Lam HY, Okina E, et al. Harnessing the tumor microenvironment: targeted cancer therapies through modulation of epithelial-mesenchymal transition. *J Hematol Oncol* *J Hematol Oncol.* 2025;18(1):6.
29. Zhao Y, Shen M, Wu L, Yang H, Yao Y, Yang Q, et al. Stromal cells in the tumor microenvironment: accomplices of tumor progression? *Cell Death Dis.* 2023;14(9):587.
30. Wang J, Peng J, Chen Y, Nasser MI, Qin H. The role of stromal cells in epithelial–mesenchymal plasticity and its therapeutic potential. *Discov Oncol.* 2024;15(1):13.

31. Lu C, Liu Y, Ali NM, Zhang B, Cui X. The role of innate immune cells in the tumor microenvironment and research progress in anti-tumor therapy. *Front Immunol.* 2023 Jan;13:1039260.
32. Anderson NM, Simon MC. The tumor microenvironment. *Curr Biol.* 2020;30(16):R921–5.
33. Baghy K, Ladányi A, Reszegi A, Kovalszky I. Insights into the Tumor Microenvironment—Components, Functions and Therapeutics. *Int J Mol Sci.* 2023;24(24):17536.
34. Huang J, Zhang L, Wan D, Zhou L, Zheng S, Lin S, et al. Extracellular matrix and its therapeutic potential for cancer treatment. *Signal Transduct Target Ther.* 2021;6(1):153.
35. Ciepła J, Smolarczyk R. Tumor hypoxia unveiled: insights into microenvironment, detection tools and emerging therapies. *Clin Exp Med.* 2024;24(1):235.
36. Semenza GL. Hypoxia-inducible factor 1: master regulator of O₂ homeostasis. *Curr Opin Genet Dev.* 1998;8(5):588–94.
37. Chen Z, Han F, Du Y, Shi H, Zhou W. Hypoxic microenvironment in cancer: molecular mechanisms and therapeutic interventions. *Signal Transduct Target Ther.* 2023;8(1):70.
38. Bigos KJA, Quiles CG, Lunj S, Smith DJ, Krause M, Troost EGC, et al. Tumour response to hypoxia: understanding the hypoxic tumour microenvironment to improve treatment outcome in solid tumours. *Front Oncol.* 2024;14:1331355.
39. Emami Nejad A, Najafgholian S, Rostami A, Sistani A, Shojaeifar S, Esparvarinha M, et al. The role of hypoxia in the tumor microenvironment and development of cancer stem cell: a novel approach to developing treatment. *Cancer Cell Int.* 2021;21(1):62.
40. Koukoulas K, Giakountis A, Karagiota A, Samiotaki M, Panayotou G, Simos G, et al. ERK signaling controls productive HIF-1 binding to chromatin and cancer cell

- adaptation to hypoxia through HIF-1 α interaction with NPM1. *Mol Oncol*. 2021;15(12):3468–89.
41. Ma Z, Xiang X, Li S, Xie P, Gong Q, Goh BC, et al. Targeting hypoxia-inducible factor-1, for cancer treatment: Recent advances in developing small-molecule inhibitors from natural compounds. *Semin Cancer Biol*. 2022;80:379–90.
 42. Zhang C, Liu J, Wang J, Zhang T, Xu D, Hu W, et al. The Interplay Between Tumor Suppressor p53 and Hypoxia Signaling Pathways in Cancer. *Front Cell Dev Biol*. 2021;9:648808.
 43. Bailey CM, Liu Y, Liu M, Du X, Devenport M, Zheng P, et al. Targeting HIF-1 α abrogates PD-L1–mediated immune evasion in tumor microenvironment but promotes tolerance in normal tissues. *J Clin Invest*. 2022;132(9):e150846.
 44. Rohwer N, Cramer T. Hypoxia-mediated drug resistance: Novel insights on the functional interaction of HIFs and cell death pathways. *Drug Resist Updat*. 2011;14(3):191–201.
 45. UCSC Xena [Internet]. 2025 [updated 2024 Aug 28; cited 2025 Febr 5]. Available from: <https://xena.ucsc.edu/UCSC Xena>
 46. Svajda L, Cserepes M, Hegyi B, Niczky T, Tóvári J. Immunomodulation in the tumor microenvironment: Therapeutic potential of combined inhibition of tumor hypoxia and PD-1/ PD-L1. *Magy Onkol*. 2024;68(2):126-135.
 47. Shirai Y, Chow CCT, Kambe G, Suwa T, Kobayashi M, Takahashi I, et al. An Overview of the Recent Development of Anticancer Agents Targeting the HIF-1 Transcription Factor. *Cancers*. 2021;13(11):2813.
 48. Viziteu E, Grandmougin C, Goldschmidt H, Seckinger A, Hose D, Klein B, et al. Chetomin, targeting HIF-1 α /p300 complex, exhibits antitumour activity in multiple myeloma. *Br J Cancer*. 2016;114(5):519–23.

49. Tanaka T, Yamaguchi J, Shoji K, Nangaku M. Anthracycline Inhibits Recruitment of Hypoxia-inducible Transcription Factors and Suppresses Tumor Cell Migration and Cardiac Angiogenic Response in the Host. *J Biol Chem*. 2012;287(42):34866–82.
50. Xu R, Wang F, Yang H, Wang Z. Action Sites and Clinical Application of HIF-1 α Inhibitors. *Molecules*. 2022;27(11):3426.
51. Martí-Díaz R, Montenegro MF, Cabezas-Herrera J, Goding CR, Rodríguez-López JN, Sánchez-del-Campo L. Acriflavine, a Potent Inhibitor of HIF-1 α , Disturbs Glucose Metabolism and Suppresses ATF4-Protective Pathways in Melanoma under Non-Hypoxic Conditions. *Cancers*. 2020;13(1):102.
52. Goldberg RM, Garrett CR, Berkowitz NC, Bekaii-Saab TS, Ryan T, Fisher GA, et al. Phase II study of EZN-2208 (PEG-SN38) with or without cetuximab in patients with metastatic colorectal cancer (CRC). *J Clin Oncol*. 2012;30(4_suppl):448–448.
53. Heath EI, Hillman DW, Vaishampayan U, Sheng S, Sarkar F, Harper F, et al. A Phase II Trial of 17-Allylamino-17-Demethoxygeldanamycin in Patients with Hormone-Refractory Metastatic Prostate Cancer. *Clin Cancer Res*. 2008;14(23):7940–6.
54. Bui BP, Nguyen PL, Lee K, Cho J. Hypoxia-Inducible Factor-1: A Novel Therapeutic Target for the Management of Cancer, Drug Resistance, and Cancer-Related Pain. *Cancers*. 2022;14(24):6054.
55. U.S. Food and Drug Administration. FDA approves belzutifan for advanced renal cell carcinoma [Internet]. 2024 [updated 2023 Dec 14; cited 2025 Febr 5]. Available from: <https://www.fda.gov/drugs/resources-information-approved-drugs/fda-approves-belzutifan-advanced-renal-cell-carcinoma>
56. Kao TW, Bai GH, Wang TL, Shih IM, Chuang CM, Lo CL, et al. Novel cancer treatment paradigm targeting hypoxia-induced factor in conjunction with current therapies to overcome resistance. *J Exp Clin Cancer Res*. 2023;42(1):171.
57. Pili R, Quinn DI, Albany C, Adra N, Logan TF, Greenspan A, et al. Immunomodulation by HDAC inhibition: Results from a phase Ib study with

- vorinostat and pembrolizumab in metastatic urothelial, renal, and prostate carcinoma patients. *J Clin Oncol*. 2019;37(15_suppl):2572–2572.
58. Rini BI, Appleman LJ, Figlin RA, Plimack ER, Merchan JR, Wang K, et al. Results from a phase I expansion cohort of the first-in-class oral HIF-2 α inhibitor PT2385 in combination with nivolumab in patients with previously treated advanced RCC. *J Clin Oncol*. 2019;37(7_suppl):558–558.
 59. Elstrodt F, Hollestelle A, Nagel JHA, Gorin M, Wasielewski M, van den Ouweland A, et al. *BRCA1* Mutation Analysis of 41 Human Breast Cancer Cell Lines Reveals Three New Deleterious Mutants. *Cancer Res*. 2006;66(1):41–5.
 60. Stordal B, Timms K, Farrelly A, Gallagher D, Busschots S, Renaud M, et al. *BRCA1/2* mutation analysis in 41 ovarian cell lines reveals only one functionally deleterious *BRCA1* mutation. *Mol Oncol*. 2013;7(3):567–79.
 61. Schrörs B, Boegel S, Albrecht C, Bukur T, Bukur V, Holtsträter C, et al. Multi-Omics Characterization of the 4T1 Murine Mammary Gland Tumor Model. *Front Oncol*. 2020;10:1195.
 62. Garay T, Kenessey I, Molnár E, Juhász É, Réti A, László V, et al. Prenylation Inhibition-Induced Cell Death in Melanoma: Reduced Sensitivity in *BRAF* Mutant/*PTEN* Wild-Type Melanoma Cells. Smalley K, editor. *PLOS ONE*. 2015;10(2):e0117021.
 63. Ianevski A, Giri AK, Aittokallio T. SynergyFinder 3.0: an interactive analysis and consensus interpretation of multi-drug synergies across multiple samples. *Nucleic Acids Res*. 2022;50(W1):W739–43.
 64. Huang DW, Sherman BT, Lempicki RA. Systematic and integrative analysis of large gene lists using DAVID bioinformatics resources. *Nat Protoc*. 2009;4(1):44–57.
 65. Huang DW, Sherman BT, Lempicki RA. Bioinformatics enrichment tools: paths toward the comprehensive functional analysis of large gene lists. *Nucleic Acids Res*. 2009;37(1):1–13.

66. Suarez-Arnedo A, Torres Figueroa F, Clavijo C, Arbeláez P, Cruz JC, Muñoz-Camargo C. An image J plugin for the high throughput image analysis of in vitro scratch wound healing assays. Chirico G, editor. PLOS ONE. 2020;15(7):e0232565.
67. Cserepes M, Nelhübel GA, Meilinger-Dobra M, Herczeg A, Türk D, Hegedűs Z, et al. EGFR R521K Polymorphism Is Not a Major Determinant of Clinical Cetuximab Resistance in Head and Neck Cancer. *Cancers*. 2022;14(10):2407.
68. Voduc D, Kenney C, Nielsen TO. Tissue Microarrays in Clinical Oncology. *Semin Radiat Oncol*. 2008;18(2):89–97.
69. Szentkereszty M, Ladányi A, Gálffy G, Tóvári J, Losonczy G. Density of tumor-infiltrating NK and Treg cells is associated with 5 years progression-free and overall survival in resected lung adenocarcinoma. *Lung Cancer*. 2024;192:107824.
70. Bankhead P, Loughrey MB, Fernández JA, Dombrowski Y, McArt DG, Dunne PD, et al. QuPath: Open source software for digital pathology image analysis. *Sci Rep*. 2017;7(1):16878.
71. Svajda L, Randelović I, Surguta SE, Baranyi M, Cserepes M, Tóvári J. Targeting hypoxia in combination with paclitaxel to enhance therapeutic efficacy in breast and ovarian cancer. *Biomed Pharmacother*. 2024;180:117601.
72. Lee CJ, Yue CH, Lin YY, Wu JC, Liu JY. Antitumor activity of acriflavine in human hepatocellular carcinoma cells. *Anticancer Res*. 2014;34(7):3549–56.
73. Hassan S, Laryea D, Mahteme H, Felth J, Fryknäs M, Fayad W, et al. Novel activity of acriflavine against colorectal cancer tumor cells. *Cancer Sci*. 2011;102(12):2206–13.
74. Shi Y, Gilkes DM. HIF-1 and HIF-2 in cancer: structure, regulation, and therapeutic prospects. *Cell Mol Life Sci*. 2025;82(1):44.
75. Wu Q, You L, Nepovimova E, Heger Z, Wu W, Kuca K, et al. Hypoxia-inducible factors: master regulators of hypoxic tumor immune escape. *J Hematol Oncol J Hematol Oncol*. 2022;15(1):77.

76. Fan J, Yang X, Bi Z. Acriflavine suppresses the growth of human osteosarcoma cells through apoptosis and autophagy. *Tumor Biol.* 2014;35(10):9571–6.
77. Pak JH, Yi J, Ryu S, Kim IK, Kim JW, Baek H, et al. Induction of Redox-Active Gene Expression by CoCl₂ Ameliorates Oxidative Stress-Mediated Injury of Murine Auditory Cells. *Antioxidants.* 2019;8(9):399.
78. Rubtsova SN, Zhitnyak IY, Gloushankova NA. Dual role of E-cadherin in cancer cells. *Tissue Barriers.* 2022;10(4):2005420.
79. Bulle A, Dekervel J, Deschuttere L, Nittner D, Van Cutsem E, Verslype C, et al. Anti-Cancer Activity of Acriflavine as Metabolic Inhibitor of OXPHOS in Pancreas Cancer Xenografts. *OncoTargets Ther.* 2020;Volume 13:6907–16.
80. Fourniols T, Bastien E, Canevat A, Feron O, Pr at V. Inhibition of colorectal cancer-associated fibroblasts by lipid nanocapsules loaded with acriflavine or paclitaxel. *Int J Pharm.* 2020;584:119337.
81. Ramesh V, Brabletz T, Ceppi P. Targeting EMT in Cancer with Repurposed Metabolic Inhibitors. *Trends Cancer.* 2020;6(11):942–50.
82. Nagelkerke A, Bussink J, Mujcic H, Wouters BG, Lehmann S, Sweep FC, et al. Hypoxia stimulates migration of breast cancer cells via the PERK/ATF4/LAMP3-arm of the unfolded protein response. *Breast Cancer Res.* 2013;15(1):R2.
83. Liu F, Yuan H, Xu C, Mao M, Feng S. Oxycodone enhances antitumor effect of paclitaxel on human breast cancer SKBR3 cells in vitro. *Clinics.* 2024;79:100458.
84. Saxena K, Jolly MK, Balamurugan K. Hypoxia, partial EMT and collective migration: Emerging culprits in metastasis. *Transl Oncol.* 2020;13(11):100845.
85. Zhang YB, Wang X, Meister E, Gong KR, Yan SC, Lu GW, et al. The Effects of CoCl₂ on HIF-1 α Protein under Experimental Conditions of Autoprogressive Hypoxia Using Mouse Models. *Int J Mol Sci.* 2014;15(6):10999–1012.

86. Kashiwagi S, Yashiro M, Takashima T, Nomura S, Noda S, Kawajiri H, et al. Significance of E-cadherin expression in triple-negative breast cancer. *Br J Cancer*. 2010;103(2):249–55.
87. Courtney KD, Infante JR, Lam ET, Figlin RA, Rini BI, Brugarolas J, et al. Phase I Dose-Escalation Trial of PT2385, a First-in-Class Hypoxia-Inducible Factor-2 α Antagonist in Patients With Previously Treated Advanced Clear Cell Renal Cell Carcinoma. *J Clin Oncol*. 2018;36(9):867–74.
88. Shen Z, Pei Q, Zhang H, Yang C, Cui H, Li B, et al. Hypoxia-inducible factor-1 α inhibition augments efficacy of programmed cell death 1 antibody in murine prostatic cancer models. *Anticancer Drugs*. 2022;33(6):587–94.
89. Gao W, Zhang X, Yang W, Dou D, Zhang H, Tang Y, et al. Prim-O-glucosylcimifugin enhances the antitumour effect of PD-1 inhibition by targeting myeloid-derived suppressor cells. *J Immunother Cancer*. 2019;7(1):231.

9. Bibliography of the candidate's publications

9.1. Publication related to the thesis

Svajda, Laura; Randelović, Ivan; Surguta, Sára Eszter; Baranyi, Marcell; Cserepes, Mihály**; Tóvári, József Targeting hypoxia in combination with paclitaxel to enhance therapeutic efficacy in breast and ovarian cancer. BIOMEDICINE & PHARMACOTHERAPY Nov:180 Paper:117601, 11 p. (2024) **IF:6.9**

9.2. Other publications

Cserepes, Mihály; Nelhübel, Györgyi A.; Meilinger-Dobra, Mónika; Herczeg, Adrienn; Türk, Dóra; Hegedűs, Zita; **Svajda, Laura**; Rásó, Erzsébet; Ladányi, Andrea; Csikó, Kristóf György; Kenessey, István; Szöőr Árpád; Vereb György; Remenár Éva; Tóvári József. EGFR R521K Polymorphism Is Not a Major Determinant of Clinical Cetuximab Resistance in Head and Neck Cancer. CANCERS 14:10 Paper:2407, 15 p. (2022) **IF:4.5**

Zambra, Marco; Randelović, Ivan*; Talarico, Francesco; Borbély, Adina; **Svajda, Laura**; Tóvári, József; Mező, Gábor; Boderó, Lizeth; Colombo, Sveva; Arrigoni, Federico et al. Optimizing the enzymatic release of MMAE from isoDGR-based small molecule drug conjugate by incorporation of a GPLG-PABC enzymatically cleavable linker FRONTIERS IN PHARMACOLOGY 14 Paper:1215694, 12 p. (2023) **IF:4.4**

Valdez Capuccino, L.; Kleitke, T.; Szokol, B.; **Svajda, L.**; Martin, F.; Bonechi, F.; Krekó, M.; Azami, S.; Montinaro, A.; Wang, Y. et al. CDK9 inhibition as an effective therapy for small cell lung cancer. CELL DEATH AND DISEASE 15:5 Paper:345, 12 p. (2024) **IF:8.1**

Surguta, Sára Eszter; Baranyi, Marcell; **Svajda, Laura**; Cserepes, Mihály; Randelović, Ivan; Tátrai, Enikő; Hegedűs, Balázs; Tóvári, József. Differential effects of hypoxia on motility using various in vitro models of lung adenocarcinoma. SCIENTIFIC REPORTS 14:1 Paper:20482, 12 p. (2024) **IF:3.8**

Svajda, Laura; Cserepes, Mihály; Hegyi, Barbara; Niczky, Theodora; Tóvári, József. Immunmoduláció a tumor mikrokozonyzetében: a tumorhipoxia és a PD-1/PD-L1

együttes gátlásának terápiás lehetőségei. MAGYAR ONKOLÓGIA 68:2 pp. 126-135.,
10 p. (2024) IF: -

10. Acknowledgments

I sincerely appreciate the invaluable support and guidance of my supervisor Dr. József Tóvári. His dedication to leadership and oncology research, along with his unwavering support and mentorship, have greatly influenced my professional growth and scientific development. I sincerely appreciate the constructive feedback and guidance provided by my co-supervisor Dr. Mihály Cserepes whose insights helped shape this work. I am deeply grateful to Attila Kigyós for his instructions, and strategic insights, which have greatly contributed to my professional growth. I wish to express my profound appreciation to the former General Director of the National Institute of Oncology, prof. Dr. Csaba Polgár, for ensuring the essential resources and infrastructure that enabled this work.

I would like to extend my heartfelt thanks to Dr. Ivan Randelović for his unwavering support and insightful advice. I am truly grateful to Sára Eszter Surguta for her professional insights, dedication, and for always being a supportive and inspiring friend throughout this journey. I sincerely appreciate Dr. Marcell Baranyi for his support, kindness, and encouragement.

A heartfelt thanks to Anita Hidvégi, Violetta Léner and Katalin Derecskei whose efficiency, and willingness to assist have been invaluable throughout these years. I would like to extend my sincere gratitude to all members of the Experimental Pharmacology Department of the National Institute of Oncology, for their hard work, dedication, and collaborative spirit.

I am endlessly grateful to my beloved family, partner, and dear friends for their unconditional love, and boundless patience. Their encouragement has been my greatest source of strength, and their faith in me has given me the confidence to persevere through every challenge.

11. Grant support

This study was funded by the National Tumor Biology Laboratory (2022-2.1.1-NL-2022-00010), the Hungarian Thematic Excellence Program (TKP2021-EGA-44), and NKFIH-OTKA grants K147410 (JT) and PD142272 (MC).